JNeurosci Accepted Manuscript

JNeurosci
THE JOURNAL OF NEUROSCIENCE

Research Articles: Development/Plasticity/Repair

The GTPase Arl8B plays a principle role in the positioning of interstitial axon branches by spatially controlling autophagosome and lysosome location

https://doi.org/10.1523/JNEUROSCI.1759-19.2020

Cite as: J. Neurosci 2020; 10.1523/JNEUROSCI.1759-19.2020

Received: 23 July 2019
Revised: 13 July 2020
Accepted: 20 July 2020

This Early Release article has been peer-reviewed and accepted, but has not been through the composition and copyediting processes. The final version may differ slightly in style or formatting and will contain links to any extended data.

Alerts: Sign up at www.jneurosci.org/alerts to receive customized email alerts when the fully formatted version of this article is published.

Copyright © 2020 the authors

JNeurosci Accepted Manuscript

The GTPase Arl8B plays a principle role in the positioning of interstitial axon branches by spatially controlling autophagosome and lysosome location

abbreviated title: Arl8B controls retinal axon branching

Gee Adnan [1], Aine Rubikaite [1], Moqadisa Khan[1], Michael Reber[2], Philip Suetterlin[1,3], Robert Hindges[1,4], and Uwe Drescher [1,4 *]

[1] Centre for Developmental Neurobiology
King's College London
New Hunts House; Guy's Campus
SE1 1UL; London, UK

[2]Krembil Research Institute
60 Leonard Ave
Toronto, ON M5T 0S8; Canada

[3]Craniofacial Development and Stem Cell Biology
King's College London
Floor 27, Tower Wing; Guy's Hospital
SE1 9RT; London, UK

[4]MRC Centre for Neurodevelopmental Disorders
King's College London
New Hunts House; Guy's Campus
SE1 1UL; London, UK

*Corresponding author
Uwe Drescher
e mail: uwe.drescher@kcl.ac.uk

Number of pages: 49
Number of Figures: 11
Number of words for Abstract: 187; Introduction: 658; and Discussion: 1320

Declaration of interests: The authors declare no competing financial interests.

Acknowledgements
We would like to thank Jon Clarke, Matthew Dawson and Manolis Fanto for instructive and insightful comments on the manuscript; Alexis Danielle Guerra (University of Irvine, California) and Regina Baranyi (KCL) for technical assistance; and Luke Smith (KCL) for reagents. The work was supported by grants to U.D. by the Royal Society (IE150445) and the BBSRC (E015522/1).

JNeurosci Accepted Manuscript

Abstract

Interstitial axon branching is an essential step during the establishment of neuronal connectivity. However, the exact mechanisms on how the number and position of branches are determined are still not fully understood. Here, we investigated the role of Arl8B, an adaptor molecule between lysosomes and kinesins. In chick retinal ganglion cells, downregulation of Arl8B reduces axon branch density and shifts their location more proximally, while Arl8B overexpression leads to increased density and more distal positions of branches. These alterations correlate with changes in the location and density of lysosomes and autophagosomes along the axon shaft. Diminishing autophagy directly by knockdown of atg7, a key autophagy gene, reduces branch density, while induction of autophagy by rapamycin increases axon branching, indicating that autophagy plays a prominent role in axon branch formation. *In vivo*, local inactivation of autophagy in the retina using a mouse conditional knockout approach disturbs retino-collicular map formation which is dependent on the formation of interstitial axon branches. These data suggest that Arl8B plays a principal role in the positioning of axon branches by spatially controlling autophagy, thus directly controlling formation of neural connectivity in the brain.

Significance statement <120 words

The formation of interstitial axonal branches plays a prominent role in numerous places of the developing brain during neural circuit establishment. We show here that the GTPase Arl8B controls density and location of interstitial axon branches, and at the same time controls also density and location of the autophagy machinery. Up- or down-regulation of autophagy *in vitro* promotes or inhibits axon branching. Local disruption of autophagy *in vivo* disturbs retino-collicular mapping. Our data suggest that Arl8B controls axon branching by controlling locally autophagy. This work is one of the first reports showing a role of autophagy during early neural circuit development and suggests that autophagy in general plays a much more prominent role during brain development than previously anticipated.

JNeurosci Accepted Manuscript

Introduction

Axonal branches, which extend interstitially from axon shafts and arborize at specific target locations, are responsible for most, if not all, neural connectivity in the vertebrate CNS (Gallo, 2011; Kalil and Dent, 2014).

The formation of interstitial branches requires cytoskeletal rearrangements at branch points. Here actin assembly often initiates filopodium formation followed by microtubule invasion which marks the maturation of the interstitial branches. Various processes have been implicated in controlling these cytoskeletal rearrangements. These include local signaling by membrane-bound receptors (e.g. EphA/ephrinAs; BDNF/TrkB) (Yates et al., 2001; Marler et al., 2008), local transport and translation of specific RNAs to sites of emerging branches (Wong et al., 2017; Cioni et al., 2019), and the capture of mitochondria (Courchet et al., 2013; Lewis et al., 2018).

In *C. elegans*, local assembly of an F-actin network initiates synapse formation and axon branching in parallel (Chia et al., 2014). Local clustering of synaptic vesicles can trigger the development of axonal branches and arborisation, as described in the synaptotropic hypothesis (Vaughn, 1989; Alsina et al., 2001; Meyer and Smith, 2006; Ruthazer et al., 2006; Cline and Haas, 2008; Matsumoto et al., 2016; Constance et al., 2018). It is not clear though which factors determine where presynaptic clusters are formed. In *C. elegans,* the small GTPase Arl8 has been shown to determine the position and number of presynaptic sites along axons of DA9 neurons (Klassen et al., 2010; Wu et al., 2013). Arl8 is also involved in the maintenance of presynaptic structures in *Drosophila*, mediating axonal co-transport of active zone (AZ) proteins and synaptic vesicle (SV) proteins in lysosome-related vesicles (Vukoja et al., 2018; Goel et al., 2019).

Arl8 belongs to the Ras superfamily of small GTP-binding proteins that switch between a membrane- and GTP-bound active form, and a cytosolic, inactive GDP-bound form (Gillingham and Munro, 2007). While members of the extended families of Arf and Arf-like (Arls) molecules participate in various

JNeurosci Accepted Manuscript

aspects of membrane organelle traffic, Arl8 is the only G protein localized specifically on lysosomes (Bagshaw et al., 2006; Garg et al., 2011; Korolchuk et al., 2011; Rosa-Ferreira and Munro, 2011; Khatter et al., 2015b).

Lysosomes are a central hub of cellular homeostasis. They degrade and recycle cell-intrinsic structures and extracellular material (Harris and Rubinsztein, 2011; Hurley and Schulman, 2014; Feng et al., 2015), and control metabolic signaling, plasma membrane repair, exocytosis, cell adhesion and migration (Pu et al., 2016). The subcellular location of lysosomes is of crucial importance for their activity (Wong and Cuervo, 2010; Korolchuk et al., 2011; Galluzzi et al., 2014; Hurley and Schulman, 2014; Pu et al., 2016; Bonifacino and Neefjes, 2017; Ferguson, 2018). For example, engulfment of cytoplasmic proteins and organelles by autophagosomes attracts lysosomes and enables their fusion to autolysosomes and the later degradation of engulfed material (e.g. Maday et al., 2012; Bento et al., 2013; Maday and Holzbaur, 2014; Filipek et al., 2017; Pu et al., 2017).

Arl8B has been identified as a key regulator of lysosome movement (for review Khatter et al., 2015a), functioning as an adaptor molecule linking lysosomes to microtubule (MT)-bound kinesin motor proteins to mediate an MT plus-end directed transport (Hofmann and Munro, 2006; Korolchuk et al., 2011; Pu et al., 2015; Niwa et al., 2016; Farias et al., 2017; Niwa et al., 2017).

Arl8B regulates not only the transport of lysosomes into axons (Farias et al., 2017; Rosa-Ferreira et al., 2018) but is also involved in their fusion with autophagosomes and late endosomes by recruiting the homotypic fusion and protein sorting (HOPS) complex (Khatter et al., 2015b; McEwan et al., 2015; Marwaha et al., 2017; Boda et al., 2019).

Here we show that Arl8B controls the positioning and density of interstitial branching of retinal ganglion cell (RGC) axons, and at the same time controls also positioning and density of lysosomes

JNeurosci Accepted Manuscript

and autophagosomes. This suggests that Arl8B plays a major role in defining the earliest stages of axon branch formation by locally controlling the dynamics of vesicles involved in autophagy.

JNeurosci Accepted Manuscript

Materials and Methods

Cloning of Arl8B expression constructs.

Chicken Arl8B cDNA was generated using primers 5'- GCCATGTTGGCGCTGCTCTC -3' and 5'-ACCTCCAGGACCTCCTGGACCTCCGCTTCTTCTAGACTTTGAATGCTG -3' from reverse transcribed chick retinal RNA as a template. This cDNA was cloned into expression vectors containing either tdTomato or GFP fluorescent proteins. Here, expression of the fusion proteins (NH_2- Arl8B-tdTomato/GFP-COOH) is under the control of the CMV and beta actin (CAG) promoter. The LAMP-YFP and the fluorescent-LC3 plasmids were purchased from Addgene (Cambridge, MA; plasmid no. 1816), and a gift of Terje Johansen (Tromso, Norway).

Mouse Arl8B cDNA was cloned from mouse brain RNA using RT-RCR into the same vectors with forward primer 5'- GCTTCTCCGGGATTTTGAGTGTTGAA -3' and reverse primer 5'-GCTTCTCCGGGATTTTGAGTGTTGAA -3'. All expression constructs generated by RT-PCR were sequence verified.

Primary chick neuronal cultures

Primary chick retinal cultures were prepared as described in Marler et al. (2008). In brief, nasal retinas were isolated from embryonic day 7 or 8 (E7 or E8) chicken embryos, dissociated to obtain a single-cell suspension and electroporated using an Amaxa Nucleofector (Lonza). Neuronal cultures were plated on poly-L-lysine (Sigma), laminin (Life Technologies) and merosine (Millipore) -coated surfaces and grown for 2 to 3 days at 37 ^{o}C in Neurobasal medium (Life Technologies), supplemented with B27 (Life Technologies), L-glutamine (Invitrogen) and forskolin (Sigma) in presence of penicillin/ streptomycin (Life Technologies).

Antibody staining

After 2 to 3 days in culture, retinal neuronal cultures were fixed using 4% paraformaldehyde (PFA), 30% sucrose in PBS, and stained for endogenous expression of Arl8B using a rabbit anti-Arl8B

JNeurosci Accepted Manuscript

159 antibody (13049-1-AP from Proteintech), which was raised by immunization with a human ARL8B
160 fusion protein.
161 In brief, after PFA fixation, cells were three times washed with 1x PBS, 0.1% Triton (PBST). For antigen
162 retrieval, cells were incubated for 1h at 60 ^{o}C in 0.1 M citrate buffer pH 6.0, and washed four times in
163 PBST, blocked in 5% BSA/ 10% donkey serum/ 0.1% Triton (Blocking buffer-1) for 2 h min at RT,
164 incubated with 1st antibody (anti-Arl8B diluted 1:100; anti-beta tubulin 1:500) in Blocking buffer-2 (1%
165 BSA; 5% donkey serum; 0.1% Triton) (for specificity control in Blocking buffer-2 only) at 4 ^{o}C
166 overnight, washed four times in PBST, incubated with anti-rabbit AlexaFluor488 antibody (1:1000);
167 anti-mouse AlexaFluor647 antibody in Blocking buffer-2 for 2 h at room temperature, washed four
168 times in PBST and stored under Mowiol. Analyses were done using a Zeiss confocal LSM800.
169 LAMP1 was stained using rabbit anti-LAMP1 antibody (Abcam ab24170). Neurons were
170 counterstained with DAPI (Roche) to visualise cell nuclei.
171
172 **Arl8B knockdown analysis**
173 For Arl8B knockdown experiments, a series of shRNAs, expressed from the U6 promoter, were
174 analyzed. These plasmids contained in addition a TagRFP expression cassette allowing the subsequent
175 identification of electroporated axons. To select (the most) efficient shRNAs, these constructs were
176 transfected together with an Arl8B-GFP expression plasmid into CHO cells or primary chick retinal
177 neurons. After two days in culture, Arl8B expression levels were determined by Western blot analysis
178 (Fig. 3) using an anti-GFP antibody (Clontech 632496). Anti-GAPDH antibody was used to normalise
179 Arl8B-GFP band intensities. Western blotting results were quantified using ImageJ and Excel
180 software.
181
182 The shRNA showing the strongest down-regulation (relative to control (scrambled) shRNAs) was used
183 for further functional characterisations. This shRNA targeted the Arl8B mRNA between nucleotides

JNeurosci Accepted Manuscript

322 and 344. ShRNAs that do not target any known mRNA ("scrambled shRNA") were used as a control in knockdown experiments.

Atg7 knockdown analysis

For ATG7 knockdown experiments, the RNA of chicken Atg7 was targeted using the miRNA- based shRNA silencing method (Shan et al., 2009). Several shRNA inserts were assembled by PCR using a series of primers including: FOR1 5'-TGCTGTAGGCTGTATGCTGAAGTCCTTGACCAATATGAACGTTTTGGCCACTGACTGAC -3', REV1 5'-AGTAACAGGCATCATACACTGAAGTCCTTGACATATGAACGTCAGTCAGTGGCCAAAAC -3', followed by FOR2 5'- ATTGCATCGATTGAAGGCTTGCTGTAGGCTGTATGCTG -3' and REV2 5'-GCAATGAATTCCAGCAATTTGTTCCATGTGAATGCTAGTAACAGGCATCATACACTG -3'. The resulting 154 nucleotide fragment was cleaved at *ClaI* and *EcoRI* restriction sites and cloned into an eGFP vector, under the control of the CAG promoter (Furukawa et al., 2011). The silencing efficiency was assessed by transfecting various constructs into CHO cells together with an Atg7-Flag expressing vector. After 3 days in culture, Atg7 expression levels were analyzed by Western blotting using an anti-FLAG antibody (Sigma F1804) (Fig. 6). As a control, a shRNA plasmid containing sequences that do not target any known mRNA ("scrambled shRNA") was used. The shRNA with the strongest knockdown efficiency (sequence shown above) was used for further experiments.

Chicken Atg7 was amplified from reverse transcribed chick retinal RNA as a template using primers 5'-AAGCTTCAATCATGGCAGCAGTCAGTAATG-3' and 5'- CTCGAGGACTGTTTCATCATCACTCATGTCC-3', cleaved at *HindIII* and *XhoI* restriction sites and cloned into the pCMV-3 Tag-3 vector (Agilent).

Experimental design and statistical analyses

The experimental design and statistical analyses are described in detail for every single Figure and experiment.

JNeurosci Accepted Manuscript

Axon branching assay

To analyse the consequences of upregulation or knockdown of Arl8B, or of Atg7, on axon branching, E7 or E8 single cell retinal cultures were electroporated with either an Arl8B-GFP expression plasmid, Arl8B (or Atg7) shRNA plasmids, GFP-RFP-LC3 (Jain et al., 2010) or control constructs. Axon branching was analyzed after 3 days in culture.

Generally, for functional knockdown/overexpression experiments, 5-10 microgram of DNA was electroporated per single cell retinal prep, for experiments to visualize particular structures (lysosomes, LC3-II puncta etc.) including co-localisation experiments , only 0.5 microgram of DNA per single cell retinal prep was electroporated.

5 ng/ml BDNF was added 24 hours after plating (Marler et al., 2008). After 3 days *in vitro*, retinal cultures were fixed and imaged by fluorescent microscopy, and axon length and branch number were analyzed using Metamorph, ImageJ (using the NeuronJ plug-in), Microsoft Excel and Graph Pad Prism software. RGCs were identified based on their neurite morphology and by immuno-cytochemical staining using RGC-specific antibodies as described in Marler et al. (2008).

Only branches longer than 5 µm were considered (Marler et al., 2008; Matsumoto et al., 2016). Branch density was determined as the number of axon branches per unit of axon length. Branch density is given as mean percentage values (normalised against the appropriate control neurons) ± standard error of the mean (S.E.M.).

All analyses were done blind to the condition. Statistical significance between the conditions was tested using Student's t- test.

Analysis of particle distribution

RGC axons expressing fusion proteins (GFP, RFP, tdTomato, mCherry) were observed using a confocal Zeiss LSM800 with a 63x objective lens. Tiles were used to capture entire RGCs and stitched using the

JNeurosci Accepted Manuscript

Carl Zeiss Microscopy software Zen 2.3 (blue edition). Z-stacks captured axonal puncta in their focal plane and were collapsed using the ImageJ tool “Z Project”.

ImageJ tools were used to analyse the proximo-distal distribution of lysosomes, autophagosomes, or synaptic vesicle clusters along RGC axons in control, Arl8B KD, Atg7 KD and other approaches (Bafilomycin, Rapamycin). The segmented line tool was used to trace the axon of each retinal ganglion cell, and the profile of pixel intensities was plotted. A background value, defined as the minimum signal value, was subtracted uniformly from each axon. The sum of pixel intensities of the proximal, middle, and distal one-third compartments was individually calculated as a percentage of the sum of pixel intensities across the axon. The mean of each one-third compartment was calculated per condition. Statistical significance between conditions was tested using Student’s t-test.

Quantification of puncta in axons – colocalisation analysis (using coloc2)

The Fiji plugin ’straighten’ is used to straighten RGC axons to exclude extracellular noise or irrelevant somatic signals. The amount of colocalisation of two fluorescent-labelled proteins in the axon is automatically quantified using the ImageJ plugin ‘Coloc 2’ (Cioni et al., 2018; Ordonez et al., 2018; Bonanomi et al., 2019). This performs pixel intensity analysis of correlation between the two channels in the straightened axon using Pearson’s linear correlation analysis, which gives a correlation coefficient value r. As a control for random overlap, Coloc2 shuffles pixel groups of one channel and repeats the correlation analysis against the second channel, giving a second r value. Coloc2 also uses the Costes method (Costes et al., 2004) to test for statistical significance between the r values (p values greater than 0.95 signify a statistical significance). The mean r value for each condition is calculated using Fisher z-transformation.

JNeurosci Accepted Manuscript

Quantification of puncta in axons – distribution of low-density puncta

For puncta that naturally occur in very low densities in the axon (such as LC3), a different method was used to quantify their distribution and density with greater accuracy. A series of ImageJ tools were used to quantify puncta density and distribution in the proximo- distal axis of individual axons. All axons were initially traced and straightened using the ImageJ tools "Segmented Line" and "Straighten" respectively. Puncta along each axon were identified using similar thresholding methods to the established Otsu method (Otsu, 1979; Matsumoto et al., 2016), namely "intermodes", which is a histogram-derived thresholding method that operates iterative smoothing until two local maxima remain. This method best identified individual puncta in proximity with each other. The plugin "Particle Analyzer" was used to quantify particles above threshold. Particles were only identified as puncta if they were larger than 2 pixels (~0.1 µm).

Particle Analyzer also allows the proximo-distal coordinates of puncta in a straightened axon to be measured. Each axon was then divided into three equal segments (proximal, middle, and distal thirds) and the coordinates of each punctum was used to quantify the number of puncta in each axon segments. The mean proportion of puncta in each axon segment was then calculated as a percentage for each condition. To calculate relative puncta density, the total number of puncta was divided by the axon length to give puncta density. Puncta densities were normalised to the mean puncta density in controls to give relative puncta density for each axon.

Quantification of density of DiI-labelled termination zones.

Whole superior colliculi (SC) of pax6-α:cre; $atg7^{fl/fl}$ mice and $atg7^{fl/fl}$ mice; cre^{-} mice were carefully dissected out and immediately imaged using a Zeiss Axioscope fluorescence microscope with a 568-nm excitation laser. A 5x objective was used to capture entire SC and any DiI-labelled termination zones (TZ).

JNeurosci Accepted Manuscript

Images were processed and TZs analyzed using ImageJ tools as follows. SCs in all images were outlined as ROI excluding all other signals. Termination zones were identified using the tool thresholding method “Triangle”, a geometric method which assumes a maximum peak in the histogram and best identifies weak TZ signals in the SC. Any background noise was identified using the remaining area of the SC which does not contain a TZ. The density of TZs was finally calculated as the raw integral values (R) minus background noise (B) divided by the area of the TZ (A), which previously was determined by thresholding (TZ density =(R – B)/A)).

The mean TZ density was calculated for each condition and significant difference was determined using an independent-samples t-test.

JNeurosci Accepted Manuscript

301 RESULTS

302 **Arl8B co-localises with lysosomes in the axonal compartment.**

303 Interstitial axon branching is a critical step during map development in the retino-tectal projection
304 (Yates et al., 2001; Hindges et al., 2002; Marler et al., 2014). Here RGC axons initially grow into the
305 tectum in a non-topographic manner and 'overshoot' their future termination zones (TZs)
306 substantially. Topographically specific interstitial branching subsequently leads to the formation of
307 TZs, and the development of a topographic map. Overshoot axon segments are later removed.
308 Members of the EphA/ephrinA family in concert with neurotrophic factors, such as BDNF and NT3,
309 play prominent roles in this branching process (for review Suetterlin et al., 2012; Cang and Feldheim,
310 2013; Weth et al., 2014).
311
312 To characterize possible roles of Arl8B in this process, the first step was to determine its subcellular
313 localisation along RGC axons. We stained retinal cultures from embryonic day (E) 8 chicks after two
314 days in culture with an Arl8B-specific antibody (see Material and Methods). This time point
315 corresponds to the major phase of retino-tectal map development between E10 and E14 during
316 which RGC axons form TZs in the tectum through intense interstitial axon branching and subsequent
317 arborisation. Our data show a punctate expression pattern throughout the RGC axonal compartment
318 (Fig. 1A and B).
319
320 As Arl8B is bound specifically to lysosomal and late endosomal membranes in vertebrate neuronal
321 and non-neuronal cells (see Introduction), we investigated whether this is also true for RGC axons. We
322 expressed an Arl8B-tdTomato fusion protein in E8 single cell retinal preparations and stained these
323 cultures three days later for LAMP1, a specific marker for lysosomes. RGCs were identified based on
324 their neurite morphology and by immuno-cytochemical staining using RGC-specific antibodies (as
325 described in Marler et al. (2008)). Super-resolution structured illumination microscopy (SIM) showed
326 an extensive co-localisation of fluorescently labelled Arl8B with LAMP1 puncta (Fig. 1C – G)

JNeurosci Accepted Manuscript

confirming that in RGC axons Arl8B associates with lysosomes. About 80% of the LAMP1 puncta were positive for Arl8B, while a small fraction of Arl8B-positive puncta was negative for LAMP1 (Fig. 1F and G). These findings are consistent with recent data from mouse hippocampal neurons (Farias et al., 2017; Vukoja et al., 2018).

A further developmental analysis showed that Arl8B protein, identified by specific antibodies, is localized in axons not only at the time of RGC branching within the tectum (Fig. 1A and 1I), but already at E6, a time when RGC axons have just reached this area (Fig. 1H), indicating a role of Arl8B beyond axon branching.

Arl8B controls the density of axon branches.

To test for a role of Arl8B in controlling interstitial axon branching, we employed both an overexpression and a knockdown approach using short hairpin RNAs (shRNAs) (Fig. 2).

In the gain of function approach, we analyzed the effects of Arl8B overexpression on axon morphology. We used here an Arl8B-GFP fusion protein which has been shown previously to be functionally intact (Korolchuk et al., 2011). Overexpression of Arl8B-GFP in cultured chick RGCs resulted in a roughly two-fold increase in axon branch density (201.1 ± 23.7% (mean ± S.E.M.)) compared to cultures transfected with control plasmid (Fig. 2A, B and D).

For the complementary knockdown approach, primary cultures from E8 chick retina were electroporated with either Arl8B shRNA plasmids (described in Fig. 3) or control shRNA constructs and analyzed by fluorescent microscopy after 3 days in culture. Knock-down of Arl8B resulted in a decrease in interstitial axon branch density (number of axonal branches per unit of axon length) to 37.6 ± 3.8% (mean ± S.E.M.) of branch density in control transfected cultures (=100%, Fig. 2A, C and

JNeurosci Accepted Manuscript

D). Arl8B knockdown had no significant effect on axon length (96.34 μm for Arl8B shRNA vs 93.17 μm for control shRNA).

Taken together, these results show that the expression level of Arl8B controls axon branch density in cultured RGCs.

Arl8B expression level affects the location of axon branches.

A crucial aspect for the development of the topographically specific formation of TZs during retino-tectal map development is where along the axon branches are formed. We therefore analyzed next whether changing Arl8B expression levels affect also the proximo-distal positioning of branches along RGC axons (Fig. 2E-I). We found that overexpression of Arl8B decreased the fraction of branches in the proximal third of axons (Fig. 2F and 2H), while a knockdown of Arl8B increases the fraction of branches formed in this area, compared with controls (Fig. 2G and 2I). Thus, after Arl8B knockdown, the fraction of branches in the proximal third rose to 169.4 ± 9.4% (mean ± S.E.M.) compared with controls (100%), while upregulation reduced the fraction of branches to 59.8 ± 5.4% (mean ± S.E.M.) of controls (Fig. 2H and 2I).

Our results therefore show that Arl8B controls the density and position of RGC axon branches, as schematized in Fig. 2J.

Characterisation of Arl8B shRNAs

To confirm their function in knocking-down Arl8B, the shRNAs used were transfected together with an Arl8B-GFP expression plasmid into Chinese Hamster Ovary (CHO) cells or primary chick retinal neurons. After two days in culture, Arl8B-GFP expression levels relative to control (scrambled) shRNA transfected cells were significantly downregulated (Fig. 3 A-D).

We used branch density as a parameter to further investigate possible off-target effects of the Arl8B shRNA, i.e. its specificity in knocking down Arl8B (Fig. 3 E-G). For this, we analyzed whether the reduced branch density mediated by the shRNA for chick Arl8B mRNA could be rescued by

JNeurosci Accepted Manuscript

overexpression of mouse Arl8B protein. A sequence alignment showed a difference in 4 out of 20 nucleotides between the shRNA target region in the chick sequence, and the corresponding region in the mouse Arl8B sequence (Fig. 3G) making it unlikely that the chick shRNA binds to mouse Arl8B mRNA. We found that overexpression of mouse Arl8B rescues the shRNA-mediated down regulation of branching (Fig. 3E). We conclude from this that the effect of the chick shRNA is specific for Arl8B and unlikely due to an off-target effect. As before, axon length was not affected by these manipulations (Fig. 3F).

Further proof for the specificity of the Arl8B shRNA was obtained by staining axons for endogenous Arl8B protein (see Materials and Methods) after shRNA transfection. We found a strong and statistically significant reduction in Arl8B-positive puncta density for Arl8B shRNA-expressing axons to about a third of the density in axons expressing the control shRNA (Fig. 3H).

Arl8B controls the density and location of lysosomes in RGC axons.

Arl8B is located on lysosomes (Fig. 1), where it promotes their anterograde transport as an adaptor molecule to kinesin motor proteins (Garg et al., 2011; Rosa-Ferreira and Munro, 2011; Tuli et al., 2013; Pu et al., 2015; Farias et al., 2017; Marwaha et al., 2017), in particular by relieving the auto-inhibition of kinesins (Niwa et al., 2016).

We therefore investigated whether the observed proximo-distal shift in relative axon branch position in response to altering Arl8B levels can be correlated with a similar shift in lysosome position (Fig. 4). Retinal cultures were transfected with expression vectors for Arl8B-GFP or control protein (GFP), together with small amounts of a LAMP1-RFP expression vector, to specifically label lysosomes. Three days later the density of LAMP1 positive puncta and their relative position along RGC axons were analyzed (Fig. 4A-G).

JNeurosci Accepted Manuscript

Our data show that Arl8B overexpression results in a roughly 2-fold overall increase in lysosome intensity compared with controls (Fig. 4E). We found a particular increase in LAMP1-RFP fluorescence in the distal axonal compartment, as well as a reduction in fluorescence in the proximal compartment (Fig. 4G). Overexpression of Arl8B did not affect axon length (Fig. 4F).
In complementary experiments (Fig. 4 H-L), we found that Arl8B knockdown reduces the overall LAMP1-GFP fluorescence in RGC axons (Fig. 4J), while axon length was not affected (Fig. 4K). Intriguingly, Arl8B knockdown increases the LAMP1-RFP fluorescence in the proximal part of axons (Fig. 4L).

In sum, underscoring its function as an adaptor molecule linking lysosomes and kinesins, we show here that overexpression of Arl8B results in an overall increase in lysosome density and their accumulation in the distal part of RGC axons, while Arl8B knockdown leads to a decrease in the density of lysosomes and their accumulation in the proximal parts of axons.

Thus, our data unravel a striking correlation between lysosome positioning and density on the one hand, and axon branch positioning and density on the other hand.

Arl8B controls autophagosome density and location.

Towards unravelling the mechanisms by which Arl8B-mediated positioning of lysosomes might play a role in positioning interstitial axon branches, we analyzed whether changing the expression level of Arl8B also affects the density or distribution of other components of the autophagy pathway (Fig. 5). For this, we expressed an mCherry-tagged version of LC3, a central protein for autophagosome biogenesis, in retinal neurons enabling us to visualize the formation of autophagosomes, a process that is considered a hallmark of induction of autophagy (Klionsky et al., 2012). The mCherry-LC3 protein normally shows a predominantly cytoplasmic and diffuse staining pattern (LC3-I), however, it

JNeurosci Accepted Manuscript

430 is (cleaved and) lipidated during autophagy induction and incorporated into forming autophagosomes
431 (LC3-II) resulting in a punctate (fluorescence) pattern (Klionsky et al., 2012). Thus, the density of
432 puncta of LC3-II can be taken as a read-out for the level of autophagy (Klionsky et al., 2012).
433 We found that expression of only mCherry-LC3 in RGC axons - that is at baseline levels of Arl8B - leads
434 to a low density of fluorescent puncta (Fig. 5A and C), indicating that RGC axons normally contain only
435 a small number of (steady-state) autophagosomes. However, after overexpression of Arl8B, we
436 observed a dramatic, roughly threefold increase in the number of fluorescent mCherry-LC3 puncta
437 (Fig. 5B and C). This increase was particularly manifest in the distal part of RGC axons, while the
438 density of puncta in the proximal part was reduced compared with controls (Fig. 5E). These findings
439 are in good agreement with other reports which showed that overexpression of Arl8B in fibroblast
440 cells leads to an increase in LC3-II levels, i.e. an increase in autophagy (Korolchuk et al., 2011).
441
442 Thus, these data show that Arl8B expression levels affect not only the spatial distribution of
443 lysosomes but also the spatial distribution of autophagosomes, such that areas of higher
444 autophagosome density are areas of higher axon branch density. This ultimately suggests that local
445 activation of autophagy is involved in branch formation.
446
447
448 **Baseline levels of autophagy are necessary for retinal axon branching**
449 Based on this intriguing correlation between Arl8B-induced axon branching and
450 autophagosome/lysosome distribution, we next asked whether abolishing or increasing autophagy
451 directly would also affect retinal axon branch density.
452
453 To study the effects of abolishing autophagy, we knocked-down Atg7, a protein whose function is
454 essential for the initiation of autophagosome formation, and which is a validated target to disrupt
455 autophagy (Komatsu et al., 2006; Komatsu et al., 2007). Using an miR-like shRNA approach (Shan et

JNeurosci Accepted Manuscript

al., 2009), we identified shRNAs which efficiently knocked-down expression of the Atg7 protein (Fig. 6 A and B). To verify that this Atg7 shRNA indeed affects autophagy, we co-transfected Atg7 shRNA and mCherry-LC3 and found a significant reduction in LC3-II puncta density compared to control shRNA transfected neurons (Fig. 6C). These results are comparable to an analysis of brain tissue from mice with a full knockout of Atg7, which showed a lack of formation of LC3-II (Komatsu et al., 2006).

In this series of experiments, we found that knockdown of Atg7 led to a reduction in overall axon branch *density* to 52.0 ± 6.52% (mean ± S.E.M.) (Fig. 6D) compared with cultures transfected with control shRNAs (100 ± 10.54% (mean ± S.E.M.)). This indicates that autophagy is affecting retinal axon branching.

Furthermore, we did not find statistically significant shifts in axon branch *location* between neurons transfected with Atg7 shRNA compared to control shRNA when investigating proximal and distal axonal thirds. In case of the proximal third, axon density in Atg7 shRNA expressing axons was reduced to 91.9 ± 13.3% (mean ± S.E.M.) of control (100% ±7.4%; p=0.608 using Student's t test)(n=11), and was slightly increased to 103.8 ± 10.1% of control (100 ± 7.5%) for the distal third (p=0.752 using Student's t test)(n=10). This suggests that global knockdown of Atg7 does not affect local axon branch location.

Axon length was not affected (Fig. 6E) suggesting that in particular the process of axon branching is sensitive to autophagy. Nevertheless, an increase in axon length after downregulation of autophagy has been observed for mouse primary cortical neurons (Ban et al., 2013), which ultimately suggests that autophagy affects different axon populations in different ways (Stavoe et al., 2016).

In a second, pharmacological approach (Fig. 7) to investigate the link between autophagy and axon branching, we used Bafilomycin-A1, a drug that prevents lysosome acidification and abolishes autophagic flow (Klionsky et al., 2012). Retinal cultures were incubated with 10 nM Bafilomycin-A1 for

JNeurosci Accepted Manuscript

the last 24 h of the 3 day-long *in vitro* culture experiments (see Materials and Methods). This treatment strongly reduced the number of axon branches per unit length (Fig. 7A), with a branch density of 41.8 ± 5.7% (mean ± S.E.M.), compared with 100 ± 0.7% (mean ± S.E.M.) branches for DMSO-treated RGC axons. In this case axon length was reduced (Fig. 7B), suggesting that Bafilomycin might have an effect also on other biological processes.

In parallel experiments, we analyzed whether Bafilomycin at the concentration tested here leads to an abolishment/reduction in autophagy in retinal cultures (Gomez-Sintes et al., 2017). For this, we analyzed again the expression level of LC3-II (Klionsky et al., 2012), however, this time using Western blot analyses (Fig. 7C and D). We found a good correlation between the concentrations of Bafilomycin-A1 in the retinal cultures and the level of LC3-II, meaning that retinal cultures at these developmental stages in fact show basal levels of autophagy (Boya et al., 2016), and that Bafilomycin-A1 abolishes autophagic flow, i.e. a prevention of acidification of lysosomes prevents their fusion with autophagosomes and thus abolishes LC3-II degradation.

Induction of autophagy increases RGC axon branching

In the complementary approach, we investigated whether increasing autophagy leads to an increase in axon branch density (Fig. 7E-G). We used an approach that is based on findings showing that an activated mTORC1 pathway blocks autophagy. Treatment of retinal cultures with Rapamycin, which inactivates the mTOR pathway, should therefore relieve this block, leading in turn to an increase in autophagy. To verify this, we transfected retinal cultures with LC3-mCherry, and analyzed the density of LC3-II positive puncta in RGC axons after treatment with Rapamycin (Fig. 7E)(see Materials and Methods). We found that overnight treatment with 20 nM Rapamycin significantly increased LC3-II puncta density in RGC axons (Fig. 7E), indicating that Rapamycin indeed increases autophagy in these cells.

JNeurosci Accepted Manuscript

Using the same experimental paradigm, we then analyzed axon branch density. Our results show that treatment with 20 nM Rapamycin overnight led to a statistically significant increase in axon branch density, compared with controls treated with DMSO only (Fig. 7F). Axon length was not affected (Fig. 7G).

Thus, our data are consistent with the idea that up- and downregulation of autophagy lead to an up- and downregulation of RGC axon branch density, respectively.

Arl8B controls axon branching through autophagy

To further scrutinize the link between Arl8B, axon branching and autophagy, we overexpressed Arl8B, but then asked whether the associated increase in axon branching (Fig. 2) could be eliminated by abolishing autophagy via knock-down of Atg7, which decreases axon branches (Fig. 6). If this decrease were not observed, it would suggest that Arl8B controls axon branching using a pathway independent of autophagy.

However, our data show in fact that the Arl8-induced increase in branch density can be abolished by a knock-down of Atg7 (Fig. 7H) and is therefore in line with our principal hypothesis that Arl8B controls axon branching via lysosome/autophagosome positioning. Additionally, overexpression of Arl8B in the presence of Rapamycin did not lead to a statistically significant increase in axon branching compared to overexpression of Arl8B alone (Fig. 7H).

Restricted co-localisation of presynaptic vesicle clusters with Arl8B-positive vesicles, autophagosomes and lysosomes.

In view of the synaptotropic hypothesis which proposes a link between axon branching and presynapse formation (see Introduction), we then analyzed a) whether presynaptic vesicle clusters co-

JNeurosci Accepted Manuscript

534 localize with Arl8B, and b) whether alterations in Arl8B expression level also shift the axonal position
535 of pre-synapses, similar to the effects shown for lysosomes (Fig. 4) and autophagosomes (Fig. 5).
536
537 To label presynaptic vesicles, we used an expression plasmid for synaptophysin tagged with GFP, syn-
538 GFP. A confocal analysis of RGC axons 2 days after transfection of small amounts of respective
539 expression plasmids showed a small co-localisation between Arl8B-tdT puncta and syn-GFP puncta
540 (Fig. 8A-C). A quantification by intensity correlation analysis using the ImageJ plugin 'coloc' (see
541 Material and Methods) demonstrates that this co-localisation shows a statistically significant
542 correlation (Pearson's correlation, r=0.45; see Materials and Methods).
543
544 Although we observed only a limited synaptophysin/Arl8B co-localisation, we investigated whether
545 presynaptic vesicle distribution would change in response to an increase or decrease in the
546 expression of Arl8B, aimed to uncover a (possible) link between positioning of presynaptic vesicle
547 clusters and axon branches. We found that a down-regulation of Arl8B using shRNA did not alter the
548 relative SV2-puncta distribution along RGC axons compared with controls (Fig. 8D and E), however, a
549 small decrease in the density of synaptophysin-positive puncta in the proximal third of axons was
550 observed after Arl8B overexpression (Fig. 8D), suggesting rather an anti-correlation between
551 positioning of presynaptic vesicle clusters and axon branching.
552
553 We also investigated a (possible) co-localisation of presynaptic vesicle clusters with lysosomes and
554 autophagosomes (Fig. 9). To monitor this, we transfected LC3-GFP into retinal cultures (Fig. 9 A-F),
555 which were then treated with Bafilomycin-A1 to increase the likelihood of detecting LC3-positive
556 puncta.
557 For all axons analyzed, we found a weak though statistically significant correlation, indicating a (small)
558 overlap between presynaptic vesicle clusters and LC3-II puncta (Pearson's correlation, r=0.46; see
559 Materials and Methods).

JNeurosci Accepted Manuscript

Similar data were obtained for a co-localisation between SV2 and lysosomes with a Pearson's correlation of r=0.12 (Fig. 9 G-L).

In sum, these studies show a rather limited co-localisation between presynaptic vesicle clusters on the one hand, and Arl8B, autophagosomes and lysosomes on the other hand. In fact, changing expression levels of Arl8B did not, or only little, affect presynaptic vesicle cluster positioning, which is in clear contrast with the obvious and consistent changes in autophagosome and lysosome positioning following Arl8B mis-expression. These results therefore suggest that Arl8B mediates its effect on axon branch density/positioning mainly through controlling (locally) autophagy-related processes but not through shifting presynaptic vesicle clusters.

Autophagy is necessary for proper formation of the retino-collicular projection

Next, we investigated whether interference with autophagy *in vivo* affects axon branching (Fig. 10), for which we used the mouse retino-collicular projection as a model, where RGC axons project from the eye to their main principle midbrain target, the superior colliculus (SC), in a topographic manner (for review Suetterlin et al., 2012; Cang and Feldheim, 2013). Based on our *in vitro* data (Fig. 6), the expectation was that blocking autophagy *in vivo* would lead to a reduction in RGC axon branching in the SC and thus a decrease in densities of the detected termination zones (TZs).

For this approach, we used a mouse line in which the atg7 gene, whose gene product is essential for autophagy and was targeted in our *in vitro* experiments (Fig. 6), can be conditionally inactivated using the cre/loxP system (Komatsu et al., 2006; Komatsu et al., 2007). These mice were crossed with a mouse line in which the Cre recombinase is expressed under control of the alpha-enhancer of the pax6 promoter whose activity is restricted to the nasal and temporal parts of the retina (alpha-pax6:cre) (Marquardt et al., 2001)). In homozygous $atg7^{fl/fl}$; cre^{+} offspring, autophagy is abolished only in these regions, leaving an unaffected area in the middle of the retina (Burbridge et al., 2014).

JNeurosci Accepted Manuscript

586 To confirm the expression of Cre in alpha-pax6:cre mice, we crossed these mice into a floxed- stop
587 tdTomato reporter line (Ai14; https://www.jax.org/strain/007914) and verified the expression of
588 tdTomato restricted to the temporal and nasal retina (Fig. 10A) and the projection pattern of
589 (tdTomato-positive) temporal and nasal RGC axons to the rostral and caudal SC respectively (Fig. 10B)
590 (Burbridge et al., 2014).
591
592 We then analyzed the offspring from crosses between heterozygous atg7$^{fl/+}$; cre^{+} mice (atg7$^{fl/+}$; cre^{+} x
593 atg7$^{fl/+}$; cre^{+}). First, we investigated retina development in the offspring from these crosses (Fig. 10C
594 – F), and found an apparently undisturbed, normal development of all retinal layers including the RGC
595 layer in atg7$^{fl/fl}$; cre $^{+}$ mice when compared to atg7$^{fl/fl}$; cre $^{-}$ mice. A quantification of the fluorescence
596 intensity of the DAPI stained RGC layer along the naso-temporal axis showed no apparent differences
597 between nasal/temporal versus central regions, neither within or between atg7$^{fl/fl}$; cre^{+} and atg7$^{fl/fl}$;
598 cre^{-} genotypes (Fig. 10E – F). This finding shows that the RGC layer contains similar numbers of cells
599 suggesting that inactivation of autophagy does not affect normal development of RGCs at least up to
600 P9.
601
602 Next, we investigated the projection pattern of nasal axons in the offspring from these crosses (Fig.
603 10G – L). For this, we injected a constant small amount of the lipophilic axon tracer DiI into the
604 peripheral part of the nasal retina at postnatal day 8 (P8). The corresponding TZs in the SC were
605 analyzed one day later at a developmental stage at which the retino-collicular projection is considered
606 to be mature (Suetterlin and Drescher, 2014). Typical images from whole mounts (Fig. 10G and H)
607 and parasagittal sections through the SC are shown (Fig. 10I and J). Using whole mount images, we
608 then quantified the density of DiI-labelled TZs, defined as the sum of pixel intensities of the TZ divided
609 by the area of the TZ (for details see Material and Methods) assuming that pixel intensity directly
610 correlates with the amount of DiI-labelled axonal branches (Fig. 10K and L).

JNeurosci Accepted Manuscript

611 Our analysis showed that the TZ density in atg7$^{fl/fl}$; cre^{+} mice (n=17) was significantly reduced to
612 53.7% +/- 7.1% (mean ± S.E.M.) when compared with controls (atg7$^{fl/fl}$; cre^{-} ; n=11; 100% +/- 17.6%
613 (mean ± S.E.M.); $p<0.05$, Fig. 10G – J). The reduction in the density of the TZs suggests that
614 inactivation of autophagy in the nasal retina results in a diminished connectivity of RGC axons in the
615 SC, which correlates well with our results obtained in *in vitro* approaches (Fig. 6).
616
617 These two sets of data support the view that the reduction in TZ branch density in atg7 $^{fl/fl}$; cre $^{+}$ mice
618 compared to atg7 $^{fl/fl}$; cre $^{-}$ mice is due to a disrupted connectivity pattern of RGC axons but not a
619 defective retina development.
620

JNeurosci Accepted Manuscript

DISCUSSION

Interstitial axon branching is a key step during the formation of neural circuits. Here we have investigated the function of the GTPase Arl8B in this process, an adaptor molecule linking lysosomes to kinesin motor proteins. We show that up and down regulation of Arl8B leads to changes in the density and position of lysosomes and autophagosomes, and this together leads to changes in axon branch density and position. Direct abolition of autophagy reduces branch density, while increasing autophagy leads to an increase in branch density. *In vivo*, disruption of autophagy in the retina leads to a disturbance of the retino-collicular projection. Our data suggest that Arl8B controls the location of axon branches by controlling positioning of lysosomes and autophagosomes, that is by controlling local autophagy.

Correlation between Arl8B-mediated location of axon branches and lysosome positioning.

Our principle finding that Arl8B, a GTPase specifically bound to lysosomes, is prominently involved in axon branch formation provides an entirely new avenue to understand the intracellular signalling controlling this process suggesting that in fact lysosomes are involved in this process.

Lysosomes exert multiple functions, and are not only involved in autophagy, but contribute to other processes including cell migration, formation of focal adhesions and membrane repair (for review Pu et al., 2016). Therefore, we characterized which of these canonical lysosome function/s are involved in controlling axon branching. For this, we demonstrate that also a direct interference with autophagy affects axon branching density, that is a decrease in autophagy reduces the density of RGC axon branches (Fig. 6), while an upregulation of autophagy increases branch density (Fig. 7). Furthermore, the Arl8B-mediated increase in branching could be abolished by knock-down of autophagy (Fig. 7H). This makes it likely that Arl8B in involved in axon branching by controlling autophagy-related lysosome functions.

JNeurosci Accepted Manuscript

Interestingly, autophagy is also required for dendritic branching (Clark et al., 2018), however, the mechanisms controlling *dendritic* branching must be different from those controlling *axonal* branching since Arl8B is not transported into dendrites (Farias et al., 2017).

An additional argument supporting our hypothesis is our finding that branching and autophagy are *locally* correlated, as visualized by the distribution of autophagosomes, which serve as a hallmark of autophagy. We found that upregulating Arl8B expression leads to an increase in lysosome and autophagosome density in the distal part of axons (Fig. 4 and 5), and therefore in the same region as we detect an increase in axon branching. Similarly, downregulation of Arl8B leads to an increased density of lysosomes in the proximal part of axons (Fig. 4) in parallel to an increase in axon branches in the same region (Fig. 2).

Arl8B controls branching via autophagosome/lysosome interactions.

How might an increased Arl8B expression lead to a higher density of autophagosomes in the distal axon? Normally, lysosomes preferentially form at the cell body and are from here transported via Arl8B/kinesins/MTs into the axon, while autophagosomes form preferentially in the distal parts of the axon (Hollenbeck, 1993; Lee et al., 2011; Maday et al., 2012; Maday and Holzbaur, 2014; Cheng et al., 2015). Autophagosomes are retrogradely transported towards the cell body only *after* their fusion with lysosomes (autophagic flow) (Maday et al., 2012). It is the fusion between lysosomes and autophagosomes which leads to an altered (activity) balance of motor proteins on these maturing autolysosomes which results in their retrograde transport back to the cell body.

After overexpression of Arl8B and in view of the function of Arl8B in relieving the kinesin autoinhibition, lysosomes appear to be linked to a much higher kinesin activity, i.e. a higher anterograde transport activity. Their fusion with autophagosomes would shift now the balance towards an anterograde transport, i.e. prevent a retrograde transport, and might therefore be the

JNeurosci Accepted Manuscript

673 reason for the higher density of autophagosomes in the distal part of axons (Fig. 5) which is linked to a
674 higher branch density.
675
676
677 **Possible mechanism of axon branch induction by local autophagy.**
678 Based on the general concept that RGC axons are normally refractory to branching, we hypothesize
679 that branching will occur only in regions where 'suppressors' of axon branching have been removed
680 by local (selective) autophagy (Fig. 11A-C). Thus, branching proceeds at locations devoid of
681 suppressors (Fig. 11D). These locations will be determined by a set of factors produced by tectal cells,
682 such as branch-promoting BDNF/TrkB and branch-suppressing EphA/ephrinA activities (Marler et al.,
683 2008) (Fig. 11).
684 Since debundling of microtubules is a defining and early feature of interstitial branching (Kalil and
685 Dent, 2014; Ketschek et al., 2015), prime intracellular targets of these combined TrkB/EphA signalling
686 cascades could be molecules which normally suppress the debundling of microtubules, such as
687 MAP1B. In support of this view it has been shown that removal of MAP1B results in an increase of
688 axon branching (Ketschek et al., 2015; Barnat et al., 2016). Moreover, the phosphorylated form of
689 MAP1B preferentially interacts with autophagosomes (Wang et al., 2006; Yue, 2007), leading to a
690 model in which the activation of upstream signalling cascades leads to the modification of the
691 suppressor MAP1B. This now becomes now a target of autophagy and is removed, which allows axon
692 branches to form and stabilize (Fig. 11).
693
694
695 **Co-localisation between Arl8B and presynaptic vesicle clusters**
696 We found a small, but significant, co-localisation between Arl8B-positive puncta (i.e. lysosomes and
697 autophagosomes) and presynaptic vesicle clusters. However, we did not observe a change in the
698 distribution of these presynapse clusters after overexpression or downregulation of Arl8B (Fig. 8) in a

JNeurosci Accepted Manuscript

699 manner suggesting a correlation with axon branching. This lack of correlation therefore does *not*
700 support a model in which presynapse formation and autophagy are entangled to control early steps of
701 axon branching.
702 On the contrary, in a restricted number of neuronal populations in *C. elegans*, axonal autophagy and
703 synapse development are functionally linked (Stavoe et al., 2016). Here mutants in genes in the
704 autophagy pathway lead to defects in synapse formation. However, this correlation was not found for
705 most other neuronal classes in *C. elegans* (Stavoe et al., 2016), and seems therefore not to be a
706 general principle of synapse formation.
707 Nevertheless, we cannot exclude that branch formation of RGC axons occurs from a sub-population of
708 pre-synaptic vesicle clusters; however, these would be difficult to detect under our experimental
709 conditions.
710
711
712 **Basal levels of autophagy are necessary for retino-collicular map formation.**
713 Little is known so far about the role of autophagy-related genes in establishing neural connectivity
714 during development *in vivo*. However, the key autophagy kinases ULK1 and ULK2 do play a role in the
715 development of the forebrain since respective knockout mutants of these genes show defects in
716 axonal pathfinding and de-fasciculation of major axonal tracts including the corpus callosum and the
717 cortico-thalamic tract (Wang et al., 2018). Defects in formation of the major forebrain commissures
718 were also observed for mutations in alfy (WDFY3), a scaffolding protein which facilitates the sorting of
719 ubiquitinated cargo into autophagosomes (Dragich et al., 2016; Napoli et al., 2018).
720 We show here now – in good agreement with our *in vitro* data – that a retina-specific knockout of
721 autophagy leads to a disturbance of the formation of the retino-collicular projection. Nasal RGC axons
722 from $atg7^{fl/fl}$; cre^{+} mice showed a significant reduction in the density of their TZs in the SC, compared
723 to $atg7^{fl/fl}$; cre^{-} controls (Fig. 11). The restricted expression of Cre in the retina but not in the SC in

JNeurosci Accepted Manuscript

724 pax6-alpha:cre mice (Fig. 11)(Marquardt et al., 2001)) allows the conclusion that these connectivity
725 defects are specifically due to a block of autophagy in RGC axons and not due to alterations in the SC.
726
727
728 Outlook
729 Our *in vitro* and *in vivo* data presented here suggest that Arl8B controls the density and positioning of
730 axon branches by regulating the transport of vesicles mediating locally autophagy. Future work will
731 focus on the identification of factors with in turn control the activity of Arl8B (Donaldson and Jackson,
732 2011; Niwa et al., 2017), the corresponding upstream signalling pathways (Marler et al., 2008), and
733 the molecular mechanisms by which autophagy controls neural circuit formation *in vivo*.
734
735
736

JNeurosci Accepted Manuscript

737 References

738

739 Alsina B, Vu T, Cohen-Cory S (2001) Visualizing synapse formation in arborizing optic axons in vivo:
740 dynamics and modulation by BDNF. Nat Neurosci 4:1093-1101.
741 Bagshaw RD, Callahan JW, Mahuran DJ (2006) The Arf-family protein, Arl8b, is involved in the spatial
742 distribution of lysosomes. Biochem Biophys Res Commun 344:1186-1191.
743 Ban BK, Jun MH, Ryu HH, Jang DJ, Ahmad ST, Lee JA (2013) Autophagy negatively regulates early axon
744 growth in cortical neurons. Mol Cell Biol 33:3907-3919.
745 Barnat M, Benassy MN, Vincensini L, Soares S, Fassier C, Propst F, Andrieux A, von Boxberg Y, Nothias
746 F (2016) The GSK3-MAP1B pathway controls neurite branching and microtubule dynamics.
747 Mol Cell Neurosci 72:9-21.
748 Bento CF, Puri C, Moreau K, Rubinsztein DC (2013) The role of membrane-trafficking small GTPases in
749 the regulation of autophagy. J Cell Sci 126:1059-1069.
750 Boda A, Lorincz P, Takats S, Csizmadia T, Toth S, Kovacs AL, Juhasz G (2019) Drosophila Arl8 is a
751 general positive regulator of lysosomal fusion events. Biochim Biophys Acta Mol Cell Res
752 1866:533-544.
753 Bonanomi D, Valenza F, Chivatakarn O, Sternfeld MJ, Driscoll SP, Aslanian A, Lettieri K, Gullo M,
754 Badaloni A, Lewcock JW, Hunter T, Pfaff SL (2019) p190RhoGAP Filters Competing Signals to
755 Resolve Axon Guidance Conflicts. Neuron 102:602-620 e609.
756 Bonifacino JS, Neefjes J (2017) Moving and positioning the endolysosomal system. Curr Opin Cell Biol
757 47:1-8.
758 Boya P, Esteban-Martinez L, Serrano-Puebla A, Gomez-Sintes R, Villarejo-Zori B (2016) Autophagy in
759 the eye: Development, degeneration, and aging. Prog Retin Eye Res 55:206-245.
760 Burbridge TJ, Xu HP, Ackman JB, Ge X, Zhang Y, Ye MJ, Zhou ZJ, Xu J, Contractor A, Crair MC (2014)
761 Visual circuit development requires patterned activity mediated by retinal acetylcholine
762 receptors. Neuron 84:1049-1064.

JNeurosci Accepted Manuscript

763 Cang J, Feldheim DA (2013) Developmental mechanisms of topographic map formation and
764 alignment. Annu Rev Neurosci 36:51-77.
765 Cheng XT, Zhou B, Lin MY, Cai Q, Sheng ZH (2015) Axonal autophagosomes recruit dynein for
766 retrograde transport through fusion with late endosomes. J Cell Biol 209:377-386.
767 Chia PH, Chen B, Li P, Rosen MK, Shen K (2014) Local F-actin network links synapse formation and
768 axon branching. Cell 156:208-220.
769 Cioni JM, Wong HH, Bressan D, Kodama L, Harris WA, Holt CE (2018) Axon-Axon Interactions Regulate
770 Topographic Optic Tract Sorting via CYFIP2-Dependent WAVE Complex Function. Neuron
771 97:1078-1093 e1076.
772 Cioni JM, Lin JQ, Holtermann AV, Koppers M, Jakobs MAH, Azizi A, Turner-Bridger B, Shigeoka T,
773 Franze K, Harris WA, Holt CE (2019) Late Endosomes Act as mRNA Translation Platforms and
774 Sustain Mitochondria in Axons. Cell 176:56-72 e15.
775 Clark SG, Graybeal LL, Bhattacharjee S, Thomas C, Bhattacharya S, Cox DN (2018) Basal autophagy is
776 required for promoting dendritic terminal branching in Drosophila sensory neurons. PLoS One
777 13:e0206743.
778 Cline H, Haas K (2008) The regulation of dendritic arbor development and plasticity by glutamatergic
779 synaptic input: a review of the synaptotrophic hypothesis. J Physiol 586:1509-1517.
780 Constance WD, Mukherjee A, Fisher YE, Pop S, Blanc E, Toyama Y, Williams DW (2018) Neurexin and
781 Neuroligin-based adhesion complexes drive axonal arborisation growth independent of
782 synaptic activity. Elife 7.
783 Courchet J, Lewis TL, Jr., Lee S, Courchet V, Liou DY, Aizawa S, Polleux F (2013) Terminal axon
784 branching is regulated by the LKB1-NUAK1 kinase pathway via presynaptic mitochondrial
785 capture. Cell 153:1510-1525.
786 Donaldson JG, Jackson CL (2011) ARF family G proteins and their regulators: roles in membrane
787 transport, development and disease. Nat Rev Mol Cell Biol 12:362-375.

JNeurosci Accepted Manuscript

788 Dragich JM, Kuwajima T, Hirose-Ikeda M, Yoon MS, Eenjes E, Bosco JR, Fox LM, Lystad AH, Oo TF,
789 Yarygina O, Mita T, Waguri S, Ichimura Y, Komatsu M, Simonsen A, Burke RE, Mason CA,
790 Yamamoto A (2016) Autophagy linked FYVE (Alfy/WDFY3) is required for establishing
791 neuronal connectivity in the mammalian brain. Elife 5.
792 Farias GG, Guardia CM, De Pace R, Britt DJ, Bonifacino JS (2017) BORC/kinesin-1 ensemble drives
793 polarized transport of lysosomes into the axon. Proc Natl Acad Sci U S A 114:E2955-E2964.
794 Feng Y, Yao Z, Klionsky DJ (2015) How to control self-digestion: transcriptional, post-transcriptional,
795 and post-translational regulation of autophagy. Trends Cell Biol 25:354-363.
796 Ferguson SM (2018) Axonal transport and maturation of lysosomes. Curr Opin Neurobiol 51:45-51.
797 Filipek PA, de Araujo MEG, Vogel GF, De Smet CH, Eberharter D, Rebsamen M, Rudashevskaya EL,
798 Kremser L, Yordanov T, Tschaikner P, Furnrohr BG, Lechner S, Dunzendorfer-Matt T, Scheffzek
799 K, Bennett KL, Superti-Furga G, Lindner HH, Stasyk T, Huber LA (2017) LAMTOR/Ragulator is a
800 negative regulator of Arl8b- and BORC-dependent late endosomal positioning. J Cell Biol
801 216:4199-4215.
802 Furukawa N, Sakurai F, Katayama K, Seki N, Kawabata K, Mizuguchi H (2011) Optimization of a
803 microRNA expression vector for function analysis of microRNA. J Control Release 150:94-101.
804 Gallo G (2011) The cytoskeletal and signaling mechanisms of axon collateral branching. Dev Neurobiol
805 71:201-220.
806 Galluzzi L, Pietrocola F, Levine B, Kroemer G (2014) Metabolic control of autophagy. Cell 159:1263-
807 1276.
808 Garg S, Sharma M, Ung C, Tuli A, Barral DC, Hava DL, Veerapen N, Besra GS, Hacohen N, Brenner MB
809 (2011) Lysosomal trafficking, antigen presentation, and microbial killing are controlled by the
810 Arf-like GTPase Arl8b. Immunity 35:182-193.
811 Gillingham AK, Munro S (2007) The small G proteins of the Arf family and their regulators. Annu Rev
812 Cell Dev Biol 23:579-611.

JNeurosci Accepted Manuscript

813 Goel P, Dufour Bergeron D, Bohme MA, Nunnelly L, Lehmann M, Buser C, Walter AM, Sigrist SJ,
814 Dickman D (2019) Homeostatic scaling of active zone scaffolds maintains global synaptic
815 strength. J Cell Biol.
816 Gomez-Sintes R, Villarejo-Zori B, Serrano-Puebla A, Esteban-Martinez L, Sierra-Filardi E, Ramirez-Pardo
817 I, Rodriguez-Muela N, Boya P (2017) Standard Assays for the Study of Autophagy in the Ex
818 Vivo Retina. Cells 6.
819 Harris H, Rubinsztein DC (2011) Control of autophagy as a therapy for neurodegenerative disease. Nat
820 Rev Neurol 8:108-117.
821 Hindges R, McLaughlin T, Genoud N, Henkemeyer M, O'Leary DD (2002) EphB forward signaling
822 controls directional branch extension and arborization required for dorsal-ventral retinotopic
823 mapping. Neuron 35.
824 Hofmann I, Munro S (2006) An N-terminally acetylated Arf-like GTPase is localised to lysosomes and
825 affects their motility. J Cell Sci 119:1494-1503.
826 Hollenbeck PJ (1993) Products of endocytosis and autophagy are retrieved from axons by regulated
827 retrograde organelle transport. J Cell Biol 121:305-315.
828 Hurley JH, Schulman BA (2014) Atomistic autophagy: the structures of cellular self-digestion. Cell
829 157:300-311.
830 Jain A, Lamark T, Sjottem E, Larsen KB, Awuh JA, Overvatn A, McMahon M, Hayes JD, Johansen T
831 (2010) p62/SQSTM1 is a target gene for transcription factor NRF2 and creates a positive
832 feedback loop by inducing antioxidant response element-driven gene transcription. J Biol
833 Chem 285:22576-22591.
834 Kalil K, Dent EW (2014) Branch management: mechanisms of axon branching in the developing
835 vertebrate CNS. Nat Rev Neurosci 15:7-18.
836 Ketschek A, Jones S, Spillane M, Korobova F, Svitkina T, Gallo G (2015) Nerve growth factor promotes
837 reorganization of the axonal microtubule array at sites of axon collateral branching. Dev
838 Neurobiol 75:1441-1461.

JNeurosci Accepted Manuscript

839 Khatter D, Sindhwani A, Sharma M (2015a) Arf-like GTPase Arl8: Moving from the periphery to the
840 center of lysosomal biology. Cell Logist 5:e1086501.
841 Khatter D, Raina VB, Dwivedi D, Sindhwani A, Bahl S, Sharma M (2015b) The small GTPase Arl8b
842 regulates assembly of the mammalian HOPS complex on lysosomes. J Cell Sci 128:1746-1761.
843 Klassen MP, Wu YE, Maeder CI, Nakae I, Cueva JG, Lehrman EK, Tada M, Gengyo-Ando K, Wang GJ,
844 Goodman M, Mitani S, Kontani K, Katada T, Shen K (2010) An Arf-like small G protein, ARL-8,
845 promotes the axonal transport of presynaptic cargoes by suppressing vesicle aggregation.
846 Neuron 66:710-723.
847 Klionsky DJ et al. (2012) Guidelines for the use and interpretation of assays for monitoring autophagy.
848 Autophagy 8:445-544.
849 Komatsu M, Wang QJ, Holstein GR, Friedrich VL, Jr., Iwata J, Kominami E, Chait BT, Tanaka K, Yue Z
850 (2007) Essential role for autophagy protein Atg7 in the maintenance of axonal homeostasis
851 and the prevention of axonal degeneration. Proc Natl Acad Sci U S A 104:14489-14494.
852 Komatsu M, Waguri S, Chiba T, Murata S, Iwata J, Tanida I, Ueno T, Koike M, Uchiyama Y, Kominami E,
853 Tanaka K (2006) Loss of autophagy in the central nervous system causes neurodegeneration
854 in mice. Nature 441:880-884.
855 Korolchuk VI, Saiki S, Lichtenberg M, Siddiqi FH, Roberts EA, Imarisio S, Jahreiss L, Sarkar S, Futter M,
856 Menzies FM, O'Kane CJ, Deretic V, Rubinsztein DC (2011) Lysosomal positioning coordinates
857 cellular nutrient responses. Nat Cell Biol 13:453-460.
858 Lee S, Sato Y, Nixon RA (2011) Lysosomal proteolysis inhibition selectively disrupts axonal transport of
859 degradative organelles and causes an Alzheimer's-like axonal dystrophy. J Neurosci 31:7817-
860 7830.
861 Lewis TL, Jr., Kwon SK, Lee A, Shaw R, Polleux F (2018) MFF-dependent mitochondrial fission regulates
862 presynaptic release and axon branching by limiting axonal mitochondria size. Nat Commun
863 9:5008.

JNeurosci Accepted Manuscript

Maday S, Holzbaur EL (2014) Autophagosome biogenesis in primary neurons follows an ordered and spatially regulated pathway. Dev Cell 30:71-85.

Maday S, Wallace KE, Holzbaur EL (2012) Autophagosomes initiate distally and mature during transport toward the cell soma in primary neurons. J Cell Biol 196:407-417.

Marler KJ, Becker-Barroso E, Martinez A, Llovera M, Wentzel C, Poopalasundaram S, Hindges R, Soriano E, Comella J, Drescher U (2008) A TrkB/EphrinA interaction controls retinal axon branching and synaptogenesis. J Neurosci 28:12700-12712.

Marler KJ, Suetterlin P, Dopplapudi A, Rubikaite A, Adnan J, Maiorano NA, Lowe AS, Thompson ID, Pathania M, Bordey A, Fulga T, Van Vactor DL, Hindges R, Drescher U (2014) BDNF promotes axon branching of retinal ganglion cells via miRNA-132 and p250GAP. J Neurosci 34:969-979.

Marquardt T, Ashery-Padan R, Andrejewski N, Scardigli R, Guillemot F, Gruss P (2001) Pax6 is required for the multipotent state of retinal progenitor cells. Cell 105:43-55.

Marwaha R, Arya SB, Jagga D, Kaur H, Tuli A, Sharma M (2017) The Rab7 effector PLEKHM1 binds Arl8b to promote cargo traffic to lysosomes. J Cell Biol 216:1051-1070.

Matsumoto N, Hoshiko M, Sugo N, Fukazawa Y, Yamamoto N (2016) Synapse-dependent and independent mechanisms of thalamocortical axon branching are regulated by neuronal activity. Dev Neurobiol 76:323-336.

McEwan DG, Popovic D, Gubas A, Terawaki S, Suzuki H, Stadel D, Coxon FP, Miranda de Stegmann D, Bhogaraju S, Maddi K, Kirchof A, Gatti E, Helfrich MH, Wakatsuki S, Behrends C, Pierre P, Dikic I (2015) PLEKHM1 regulates autophagosome-lysosome fusion through HOPS complex and LC3/GABARAP proteins. Mol Cell 57:39-54.

Meyer MP, Smith SJ (2006) Evidence from in vivo imaging that synaptogenesis guides the growth and branching of axonal arbors by two distinct mechanisms. J Neurosci 26:3604-3614.

Napoli E, Song G, Panoutsopoulos A, Riyadh MA, Kaushik G, Halmai J, Levenson R, Zarbalis KS, Giulivi C (2018) Beyond autophagy: a novel role for autism-linked Wdfy3 in brain mitophagy. Sci Rep 8:11348.

JNeurosci Accepted Manuscript

890 Niwa S, Lipton DM, Morikawa M, Zhao C, Hirokawa N, Lu H, Shen K (2016) Autoinhibition of a
891 Neuronal Kinesin UNC-104/KIF1A Regulates the Size and Density of Synapses. Cell Rep
892 16:2129-2141.
893 Niwa S, Tao L, Lu SY, Liew GM, Feng W, Nachury MV, Shen K (2017) BORC Regulates the Axonal
894 Transport of Synaptic Vesicle Precursors by Activating ARL-8. Curr Biol 27:2569-2578 e2564.
895 Ordonez DG, Lee MK, Feany MB (2018) alpha-synuclein Induces Mitochondrial Dysfunction through
896 Spectrin and the Actin Cytoskeleton. Neuron 97:108-124 e106.
897 Otsu N (1979) A Threshold Selection Method from Gray-Level Histograms. IEEE TRANSACTIONS ON
898 SYSTREMS, MAN, AND CYBERNETICS 9.
899 Pu J, Keren-Kaplan T, Bonifacino JS (2017) A Ragulator-BORC interaction controls lysosome positioning
900 in response to amino acid availability. J Cell Biol 216:4183-4197.
901 Pu J, Guardia CM, Keren-Kaplan T, Bonifacino JS (2016) Mechanisms and functions of lysosome
902 positioning. J Cell Sci 129:4329-4339.
903 Pu J, Schindler C, Jia R, Jarnik M, Backlund P, Bonifacino JS (2015) BORC, a multisubunit complex that
904 regulates lysosome positioning. Dev Cell 33:176-188.
905 Rosa-Ferreira C, Munro S (2011) Arl8 and SKIP act together to link lysosomes to kinesin-1. Dev Cell
906 21:1171-1178.
907 Rosa-Ferreira C, Sweeney ST, Munro S (2018) The small G protein Arl8 contributes to lysosomal
908 function and long-range axonal transport in Drosophila. Biol Open 7.
909 Ruthazer ES, Li J, Cline HT (2006) Stabilization of axon branch dynamics by synaptic maturation. J
910 Neurosci 26:3594-3603.
911 Shan Z, Lin Q, Deng C, Li X, Huang W, Tan H, Fu Y, Yang M, Yu XY (2009) An efficient method to
912 enhance gene silencing by using precursor microRNA designed small hairpin RNAs. Mol Biol
913 Rep 36:1483-1489.
914 Stavoe AK, Hill SE, Hall DH, Colon-Ramos DA (2016) KIF1A/UNC-104 Transports ATG-9 to Regulate
915 Neurodevelopment and Autophagy at Synapses. Dev Cell 38:171-185.

JNeurosci Accepted Manuscript

916 Suetterlin P, Drescher U (2014) Target-independent ephrinA/EphA-mediated axon-axon repulsion as a
917 novel element in retino-collicular mapping Neuron 84:1-13.
918 Suetterlin P, Marler KM, Drescher U (2012) Axonal ephrinA/EphA interactions, and the emergence of
919 order in topographic projections. Semin Cell Dev Biol 23:1-6.
920 Tuli A, Thiery J, James AM, Michelet X, Sharma M, Garg S, Sanborn KB, Orange JS, Lieberman J,
921 Brenner MB (2013) Arf-like GTPase Arl8b regulates lytic granule polarization and natural killer
922 cell-mediated cytotoxicity. Mol Biol Cell 24:3721-3735.
923 Vaughn JE (1989) Fine structure of synaptogenesis in the vertebrate central nervous system. Synapse
924 3:255-285.
925 Vukoja A, Rey U, Petzoldt AG, Ott C, Vollweiter D, Quentin C, Puchkov D, Reynolds E, Lehmann M,
926 Hohensee S, Rosa S, Lipowsky R, Sigrist SJ, Haucke V (2018) Presynaptic Biogenesis Requires
927 Axonal Transport of Lysosome-Related Vesicles. Neuron 99:1216-1232 e1217.
928 Wang B, Iyengar R, Li-Harms X, Joo JH, Wright C, Lavado A, Horner L, Yang M, Guan JL, Frase S, Green
929 DR, Cao X, Kundu M (2018) The autophagy-inducing kinases, ULK1 and ULK2, regulate axon
930 guidance in the developing mouse forebrain via a noncanonical pathway. Autophagy 14:796-
931 811.
932 Wang QJ, Ding Y, Kohtz DS, Mizushima N, Cristea IM, Rout MP, Chait BT, Zhong Y, Heintz N, Yue Z
933 (2006) Induction of autophagy in axonal dystrophy and degeneration. J Neurosci 26:8057-
934 8068.
935 Weth F, Fiederling F, Gebhardt C, Bastmeyer M (2014) Chemoaffinity in topographic mapping
936 revisited - Is it more about fiber-fiber than fiber-target interactions? Semin Cell Dev Biol
937 35C:126-135.
938 Wong E, Cuervo AM (2010) Integration of clearance mechanisms: the proteasome and autophagy.
939 Cold Spring Harb Perspect Biol 2:a006734.

JNeurosci Accepted Manuscript

940 Wong HH, Lin JQ, Strohl F, Roque CG, Cioni JM, Cagnetta R, Turner-Bridger B, Laine RF, Harris WA,
941 Kaminski CF, Holt CE (2017) RNA Docking and Local Translation Regulate Site-Specific Axon
942 Remodeling In Vivo. Neuron 95:852-868 e858.
943 Wu YE, Huo L, Maeder CI, Feng W, Shen K (2013) The Balance between Capture and Dissociation of
944 Presynaptic Proteins Controls the Spatial Distribution of Synapses. Neuron 78:994-1011.
945 Yates PA, Roskies AL, McLaughlin T, O'Leary DD (2001) Topographic-specific axon branching controlled
946 by ephrin-as is the critical event in retinotectal map development. J Neurosci 21:8548-8563.
947 Yue Z (2007) Regulation of neuronal autophagy in axon: implication of autophagy in axonal function
948 and dysfunction/degeneration. Autophagy 3:139-141.
949
950
951
952

JNeurosci Accepted Manuscript

953 **Figure legends**

954

955 **Figure 1. Arl8B is expressed on RGC axons and co-localizes here with LAMP1 positive lysosomes.**

956 (A) Neuronal cultures derived from E8 chicken retinae were incubated for 2 days and stained with an
957 antibody against Arl8B. Analysis of RGCs shows a punctate staining along the axon. (B) Control
958 staining (omitting 1st antibody) of an RGC axon. Representative examples are shown. Conditions for
959 image acquisition and data processing were identical for (A) and (B).
960 Scale bar: 5 μm.
961 (C – E) Co-localisation of LAMP1-positive lysosomes (C) with Arl8B-tdT (D). Single cells from an E8
962 dissociated retina preparation were electroporated with an Arl8B-tdTomato (Arl8B-tdT) expression
963 construct and incubated for 3 days in culture. Lysosomes were identified by staining with an anti-
964 LAMP1 antibody. Insets (C' – E') show higher magnifications of boxed areas to highlight co-
965 localisations. These analyses were done by super resolution SIM.
966 Scale bar: 10 μm.
967 (F) Profile plots of (C) and (D) in which peaks represent the position of puncta along the axon. (G)
968 Venn diagram indicating the percentage of co-localisation between Arl8-tdT and LAMP1–positive
969 puncta, with 80% LAMP1 puncta positive for Arl8B, and 59% Arl8B puncta positive for LAMP1.
970 (H) and (I) Endogenous expression pattern of Arl8B at developmental time points E6 and E9. Scale bar:
971 5 μm.

972

973

974 **Figure 2. Arl8B controls RGC axon branch density and position.**

975 E8 chick single retinal cells were electroporated with expression constructs to either knockdown or to
976 overexpress Arl8B. After 3 days in culture, neurons were fixed, and RGC axon length and branch
977 number determined. Branch density is given as the number of axon branches per unit axon length.
978 The values were normalised against cultures expressing corresponding control constructs. Axon

JNeurosci Accepted Manuscript

length and branch number were analyzed using Metamorph and NeuronJ. For each experimental condition, three independent experiments were performed with n>15 axons for each experiment.

(A – D) After knockdown or overexpression of Arl8B, the density of RGC axon branches was determined.
(A – C) Representative images of RGC axons from (A) control, (B) Arl8B overexpression, and (C) Arl8B shRNA knockdown. (D) Quantification of branch counts in the different conditions. Arl8B overexpression increases the number of axon branches by a factor of about 2 (to 201.1 ± 23.7 %; control 100%), while Arl8B knockdown decreased axon branching by about two-thirds to 37.6 ± 3.8 %. The characterisation of Arl8B shRNA including rescue experiments are shown in Fig. 3. Scale bar in A – C 5 μm.

(E – I) Determination of the proximo-distal location of RGC axon branches after knockdown or overexpression of Arl8B.
(E – G) Representative images of RGC axons from control cultures (E), Arl8B overexpression (F), and Arl8B shRNA knockdown (G).
(H) Arl8B overexpression decreased axon branching to 59.8 ± 5.4% in the proximal third, while (I) Arl8B shRNA knockdown increased the fraction of axon branches in the proximal third to 169.4 ± 9.4% (control=100% ± 9%).

Statistical analysis was performed using Student's t-test. Error bars denote S.E.M. and significance is indicated as *** with $p<0.001$, and * with $p<0.05$. Scale bar in (E – G) represents 5 μm.

(J) Schematic summary of the results from overexpression and knock-down of Arl8B on RGC branch location and number.

JNeurosci Accepted Manuscript

Figure 3. Characterisation of shRNAs for chick Arl8B knockdown and rescue experiments.

(A – D) Arl8-GFP together with either an shRNA specific for Arl8B or a control (scrambled) shRNA were co- electroporated into CHO cells (A, B) or E8 retinal cultures (C, D). Two days later, cell lysates were investigated in a Western blot analysis using an anti-GFP antibody and for a loading control, an anti-GAPDH antibody (A, C). The corresponding quantifications are shown in (B) and (D). Data shown are the result of three (A, B) or two (C, D) independent experiments. IB: immunoblot.

(E – G) To demonstrate the specificity of the chick arl8B shRNA, rescue experiments were performed using mouse Arl8B expression constructs. The downregulation of branching density by the shRNA specific for chick Arl8B is fully rescued by overexpression of mouse Arl8B (E). Axon length is not affected in these experiments (F). A sequence comparison shows 4 nucleotide differences in the relevant mouse sequence compared to the chick shRNA target sequence (G).

(H) The density of endogenous Arl8B puncta in chick RGC axons is significantly downregulated after Arl8B shRNA transfection.

N numbers shown within the bars (E – F; H) indicate the number of axons analyzed. Error bars represent S.E.M. The statistical significance is given with *: $p<0.05$, and **: $p<0.01$ using Student's t-test.

Figure 4. Modulation of Arl8B expression affects density and position of lysosomes in RGC axons.

(A – D) Retinal cultures were transfected with expression plasmids for Arl8B-GFP (A-B, B') or GFP (C-D, D'), and small amounts of LAMP1-RFP (A-D) to visualize lysosome distributions. After 3 days in culture, neurones were analyzed for LAMP1-RFP fluorescence intensity and distribution (E – G). The sum of three independent experiments is shown.

(B') and (D') represent higher magnifications of axonal segments from (B) and (D) respectively, to illustrate the increase in lysosome density in the distal axon after Arl8B-GFP overexpression.

JNeurosci Accepted Manuscript

Overexpression of Arl8B-GFP results in a significant increase in the intensity of LAMP1-RFP (E). Axon length is not affected (F). Lysosome-RFP intensity is decreased in the proximal third of axons, while it is increased in the distal third (G).

(H-L) Retinal cultures were transfected with control shRNA (H) or Arl8B shRNA (I), together with small amounts of LAMP1-GFP (H,I) to visualize lysosome distributions. Cultures were fixed 3 days later and analyzed for LAMP-1-GFP fluorescence distribution along the axons.
A quantification of the LAMP1-GFP distribution is given in (J-L). Arl8B knockdown results in a significant reduction in the overall intensity of LAMP1-GFP fluorescence (J), and a fluorescence shift to the proximal third of axons (L). Axon length is not affected (K).
The quantification method used is described in Methods.
Statistical analysis was performed using Student's t-test. Error bars denote S.E.M. and significance is indicated as * with $p<0.05$, and *** with $p<0.001$; n.s. not significant. The number of axons analyzed (n) is given within the columns. Scale bars 20 μm for A-D, and 10 μm for H-I.
CB: cell body

Figure 5. Arl8B controls autophagosome density and position.

Single cell retinal cultures were transfected with expression constructs for either GFP (A, control) or Arl8B-GFP (B), together with small amounts of mCherry-LC3, and analyzed 3 days later for density and distribution of LC3-II puncta. Inserts (A' and B') represent higher magnifications of the distal part of the axons boxed in (A) and (B) respectively. Overexpression of Arl8B leads to a roughly 3-fold increase in the density of puncta (C), while axon length is unaffected (D). Arl8B overexpression leads to a higher density of puncta in the distal third of axons, and a lower density in the proximal part compared to control (E).

JNeurosci Accepted Manuscript

Data summarize the results of two independently carried out experiments. The total number of axons analyzed (n) is given within the bars.

(C – E) Error bars denote S.E.M. Statistical analyses were done using Student's t-test. ***with p <0.001; * with p<0.05; n.s. not significant. (A and B) scale bar 10 μm.

Figure 6. Autophagy controls axon branching.

Increasing or decreasing autophagy results in an increase or decrease in RGC axon branch density, respectively.

(A and B) Characterisation of shRNAs for ATG7. (A) Plasmids for expression of $Atg7^{Flag}$, and either Atg7 shRNA or a control (scrambled) shRNA plasmids were co-transfected into CHO cells. Three days later, the lysates were investigated in a Western blot analysis using an anti-FLAG antibody and for a loading control, an anti-alpha-tubulin antibody.

(B) Corresponding quantification from three independent experiments. Error bars represent S.E.M.

(C – E) Single cell cultures from E8 dissociated chick retina were transfected with shRNAs against Atg7 to block autophagy, or with a control shRNA. (C) Analysis of retinal cultures after transfection of Atg7 shRNA and a plasmid for GFP-LC3 shows a downregulation of LC3-II puncta density compared to transfection with control shRNAs. (D) Reduction in axon branch density in axons transfected with Atg7 shRNA compared to controls. Axon length was not affected (E).

(C – E) Error bars denote S.E.M. Statistical analyses were done using Student's t-test. *** with p <0.001; * with p<0.05; n.s. not significant.

JNeurosci Accepted Manuscript

Figure 7. Pharmacological interference with autophagy affects axon branch density.

(A) Axon branch density is reduced after incubation of retinal cultures with 10 nM Bafilomycin-A1 for the last 24 h of 3 day-long experiments. (B) Under the same conditions, axon length is downregulated. (C) Western blot analysis of the expression levels of LC3-II, as an indicator for the block of autophagic flow triggered by Bafilomycin-A1. GAPDH expression levels were determined as loading control. The Western blot image shows a representative of four independent experiments. (D) corresponding quantification of band intensity (LC3-II) relative to GAPDH band intensity derived from 4 independent experiments.

(E - G) Treatment of retinal cultures with 20 nM Rapamycin results in an increase in LC3-II puncta density (E), and a more than 2-fold increase in axon branch density (F). Thus, the increase in autophagosome density indicates an increase in autophagy induction via a Rapamycin-induced block of the mTOR pathway which normally inhibits autophagy (see Text for details). Axon length was not affected (G).

(H) Arl8B exerts its effect on axon branching via autophagy-related pathways. Arl8B overexpression (OE) on its own results in an increase in branch density, while knock-down (KD) of Atg7 (abolishing autophagy) on its own leads to a decrease in branching. When combined, the Arl8-induced increase in branch density is abolished by the Atg7 known-down suggesting that Arl8B exerts its effect on axon branching via an autophagy-related pathway. Overexpression of Arl8B in the presence of Rapamycin to activate autophagosome formation results in a statistically insignificant increase in branch density compared to Arl8B OE only. The sum of results of two independent experiments is shown.

Error bars denote S.E.M. Statistical analyses were done using Student's t-test. ***: $p < 0.001$; **: $p < 0.01$; *: $p < 0.05$; n.s.: not significant. Data summarize the results of four (C and D), three (A and B) or

JNeurosci Accepted Manuscript

two (E – G, H) independently carried out experiments. The total number of axons analyzed (n) is given within the bars.

Figure 8. Limited co-localisation between Arl8B and presynaptic vesicle clusters.

(A-C) For a co-localization analysis, very small amounts of Arl8B-tdTomato and synaptophysin-GFP were transfected into single cell retinal cultures, and investigated 3 days later. (A) Arl8B-tdTomato, (B) synaptophysin-GFP, (C) merger of (A) and (B). See text for a quantitative description of the limited overlap between Arl8B and synaptophysin.

(D) Distribution of synaptophysin-GFP positive puncta along RGC axons after overexpression of Arl8B (using large amounts of Arl8B-GFP) or GFP (control). The presynaptic vesicle clusters were visualized by transfection of small amounts of synaptophysin-GFP.

(E) Little changes in the distribution of synaptophysin-GFP positive puncta along RGC axons after Arl8B knockdown, in comparison to control shRNA.

Error bars denote S.E.M. Statistical analyses were done using Student's t-test. *: $p < 0.05$; n.s.: not significant. Data summarize in each case the results of two independently carried out experiments. The total number of axons analyzed (n) is given within the bars.

Figure 9. Limited co-localisation of autophagosomes and lysosomes with presynaptic vesicle clusters on RGC axons.

(A – F) Cultures prepared from E8 chick retina were transfected with small amounts of plasmids for GFP-LC3 expression to visualise LC3-II puncta (autophagosome) formation (C), incubated for 3 days and stained for SV2 to identify presynaptic vesicle clusters (B). (A) shows the morphology of the RGC of interest. (D) merger of (B) and (C). An area of partial co-localisation between a presynaptic vesicles

JNeurosci Accepted Manuscript

cluster and a LC3-II punctum is shown enlarged in insets of (B-D). ImageJ 'coloc' programs show a small but significant overlap between SV2 and LC3 positive puncta (see text and Methods for details). (E) and (F) Graphical representations of pixel intensity of (B) and (C). Areas of partial or full co-localisation are indicated by vertical lines between (E) and (F).

(G – L) Similar to experiments described in (A – F), retinal cultures were transfected with small amounts of synaptophysin-GFP (SV2-GFP; H) and LAMP1-RFP (I), to analyse co-localisations between presynaptic vesicle clusters and lysosomes (J). (G) shows a scheme of the morphology of the RGC of interest. Insets in (H) to (J) highlight an area of partial co-localisation between lysosomes and presynaptic vesicle clusters.

(K) and (L) show graphical representations of pixel intensity of (H) and (I). Areas of partial or full co-localisation are indicated by vertical lines between (K) and (L).

Figure 10. A retina-specific knockout of autophagy disrupts retino-collicular map development.

(A and B) To demonstrate the restricted Cre expression in pax6-alpha:cre mice, the projection pattern of RGC axons was analyzed in a cross with Ai14 mice expressing tdTomato in a cre-dependent manner.

(A) Flat-mounted retina at P7 showing a typical Cre-negative central dorso-ventral corridor (arrow) within an otherwise tdTomato-positive retina. The nasal cut (during preparation to orient the retina) is indicated by an arrowhead. Part of the temporal retina was omitted during preparation. (B) dorsal view of a whole mount of a typical SC, showing a tdTomato-negative central corridor (arrow) along the dorso-lateral axis within an overall tdTomato-positive SC. The slight staining in the central corridor is due to axons crossing this area in the deeper SC layers eventually invading and forming TZs in the superficial part of the caudal/posterior SC.

JNeurosci Accepted Manuscript

(C - F) DAPI staining of horizontal sections of representative retinae of atg7$^{fl/fl}$; cre^{-} (C) and atg7$^{fl/fl}$; cre^{+} (D) mice show undisturbed RGC layer formation in atg7$^{fl/fl}$; cre^{+} mice. Arrows denotes the RGC layer.

(E – F) Quantification of fluorescence intensity of the RGC layer (as an indication of the number of cell nuclei; RGC layer labelled in (C) and (D) with arrows) along the naso-temporal axis from 5 random different sections show no apparent differences between nasal/temporal versus central regions, neither within or between atg7$^{fl/fl}$; cre^{+} and atg7$^{fl/fl}$; cre^{-} genotypes. The dotted line indicates the average of all 5 densities.

(G – L) Analysis of TZs of nasal RGC axons from either atg7$^{fl/fl}$; cre^{+} or atg7$^{fl/fl}$; cre^{-} mice. DiI was focally injected in the nasal periphery of P8 offspring from atg7$^{fl/+}$; cre^{+} x atg7$^{fl/+}$; cre^{+} crosses, and fluorescence microscopy of SC whole mounts (G and H) was carried out one day later. Representative images from both genotypes of TZs in the posterior part of the SC are shown (same orientation as in (B)). Overall the TZs in atg7$^{fl/fl}$; cre^{+} (H) appear weaker than in corresponding atg7$^{fl/fl}$; cre^{-} controls (G). (I and J) Parasagittal sections to further analyse TZs. Arrows indicate the rostral and caudal borders of the SC. Sections in (I and J) are from different SCs than the whole mounts shown in (G) and (H). Analysis was done blind to genotype.

(K and L) Quantification of TZ densities in atg7$^{fl/fl}$; cre^{+} and atg7$^{fl/fl}$; cre^{-} mice (see Materials and Methods). Densities of TZs in individual mice are shown in (K), and the sum for each genotype is shown in (L). The number of mice analyzed is given within the columns (L). The difference in densities between the two genotypes is statistically significant with *: $p < 0.05$.

Error bars denote S.E.M. Statistical analyses were done using Student's t-test. * with $p<0.05$. Data summarize the results of two series of independently carried out injections. The total number of mice analyzed (n) is given within the bars.

C: caudal; D: dorsal; N: nasal; R: rostral; T: temporal; V: ventral

JNeurosci Accepted Manuscript

Fig. 11. A model for axon branch induction by local autophagy.

(A) An axon in its basic state is refractory to branch formation due to the presence of a hypothesized branch-supressing activity (suppressor).

(B) Locally acting branching factor/s modify this suppressor/s (-P). For RGC axons, good candidates are BDNF/TrkB as branch promoting and EphA/ephrinAs as branch-suppressing activities, which have been shown to interact (Marler et al., 2008) and whose balance might be crucial for the local formation of branches.

(C) The modified suppressor/s are targeted by autophagosomes, which subsequently fuse with lysosomes, mediated by Arl8B.

(D) The local removal of branch suppressors allows the local formation of branches.

MT: microtubules.

JNeurosci Accepted Manuscript

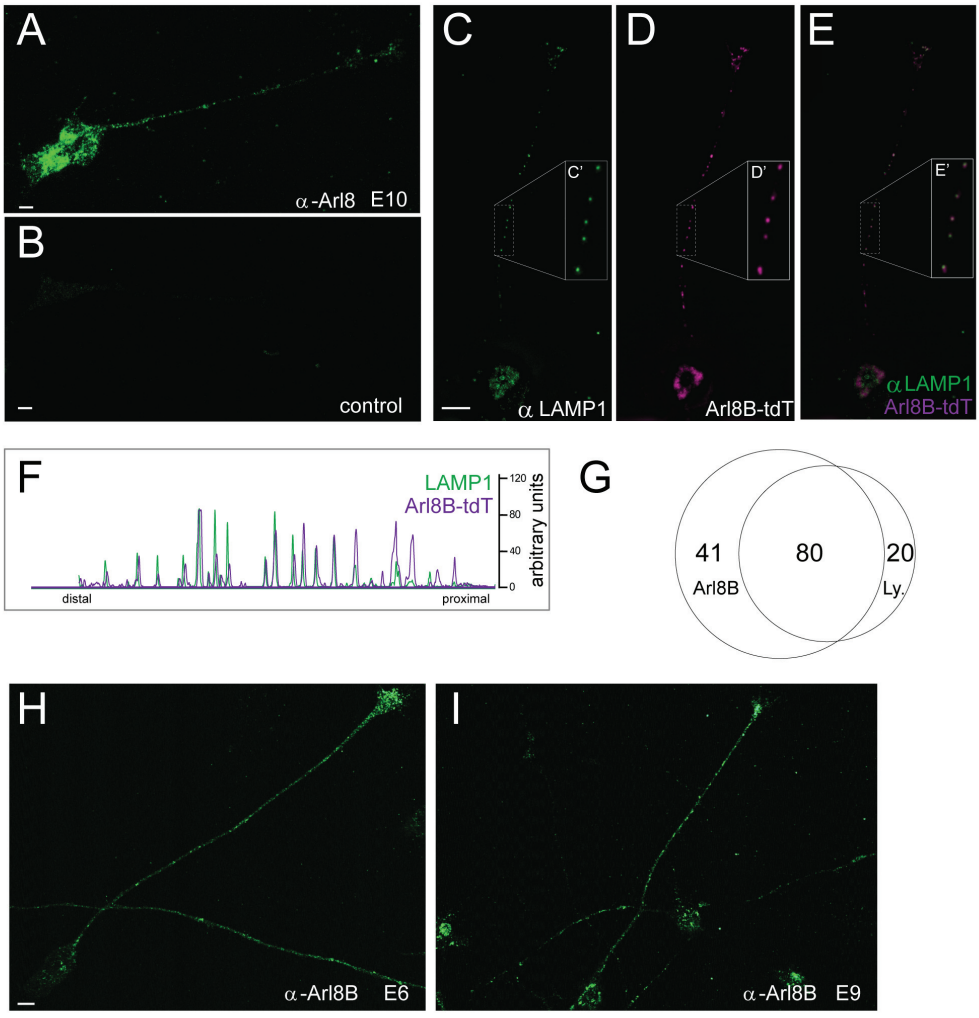

Figure 1

JNeurosci Accepted Manuscript

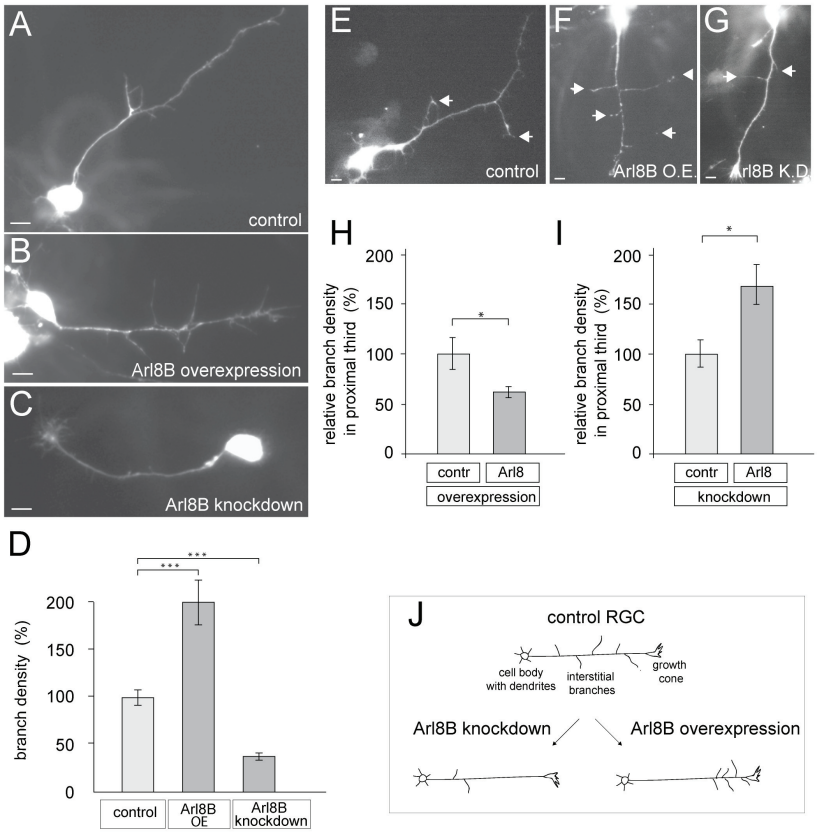

Figure 2

JNeurosci Accepted Manuscript

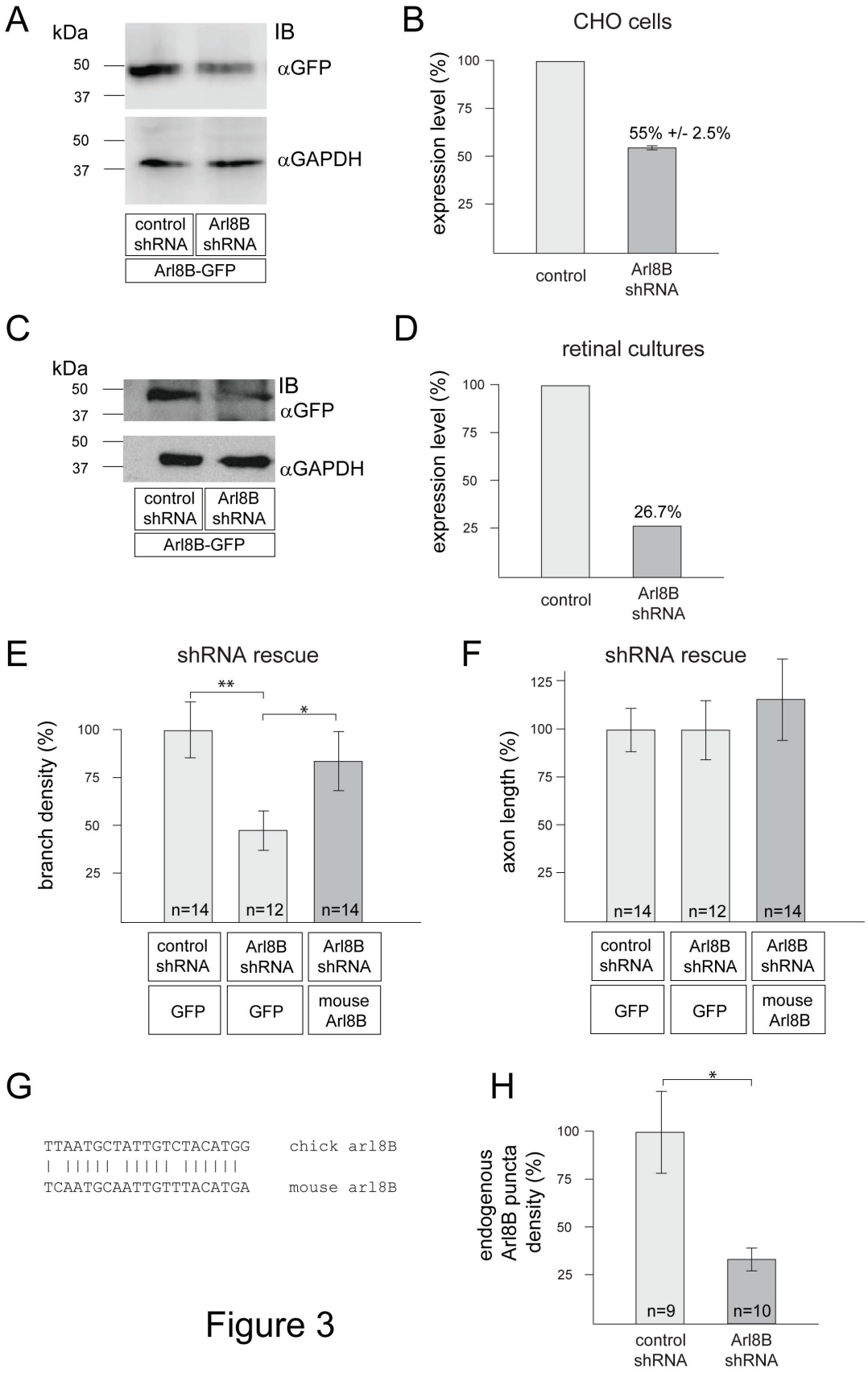

Figure 3

JNeurosci Accepted Manuscript

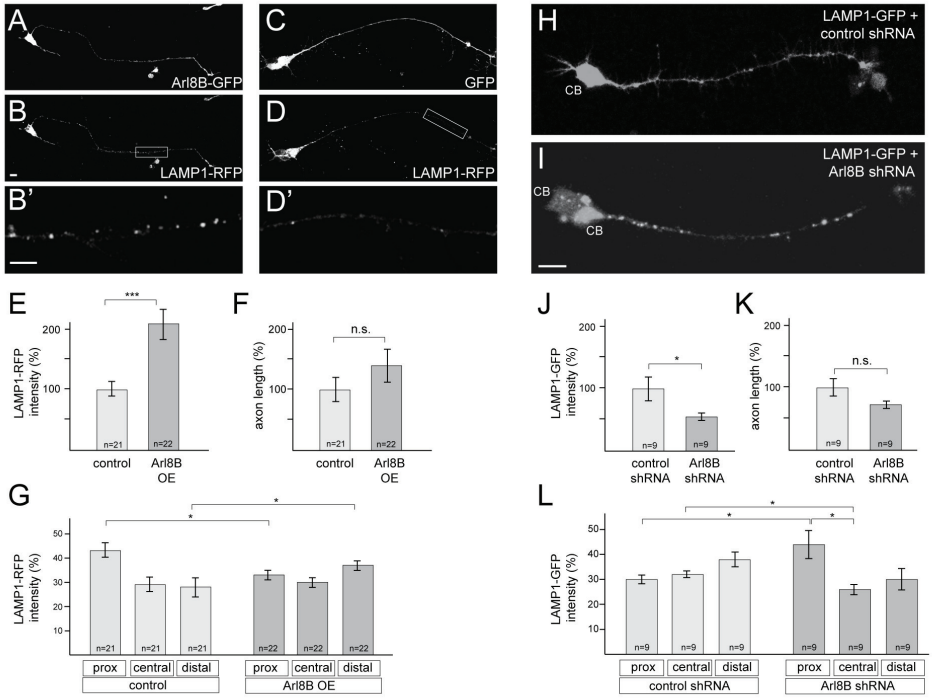

Figure 4

JNeurosci Accepted Manuscript

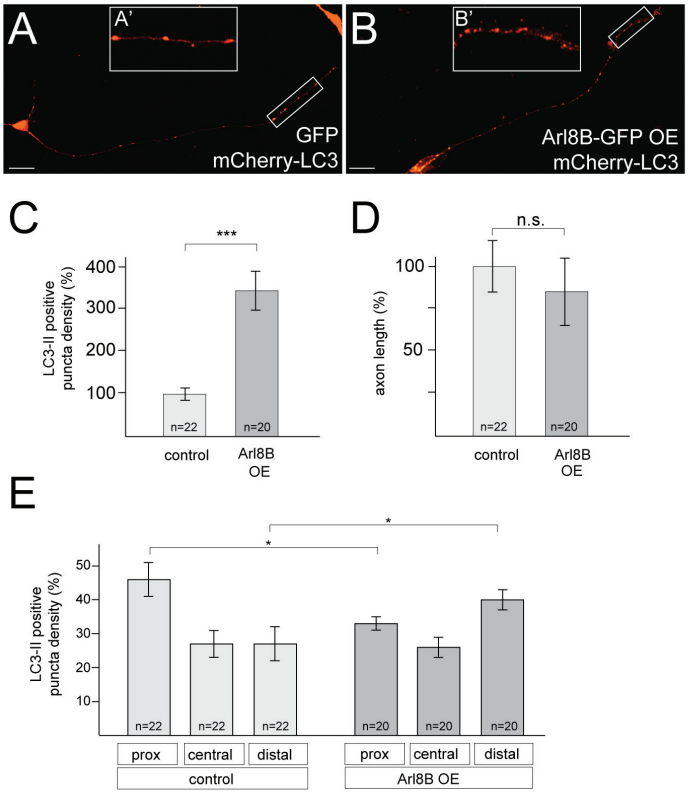

Figure 5

JNeurosci Accepted Manuscript

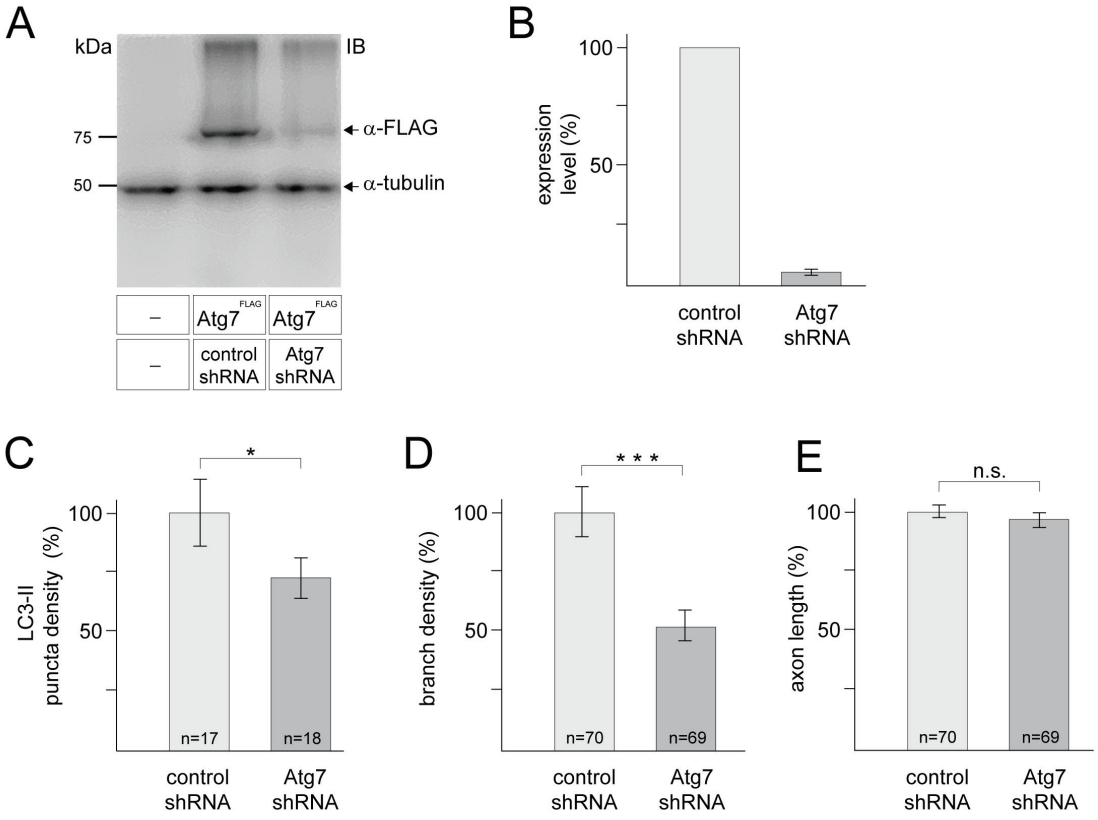

Figure 6

JNeurosci Accepted Manuscript

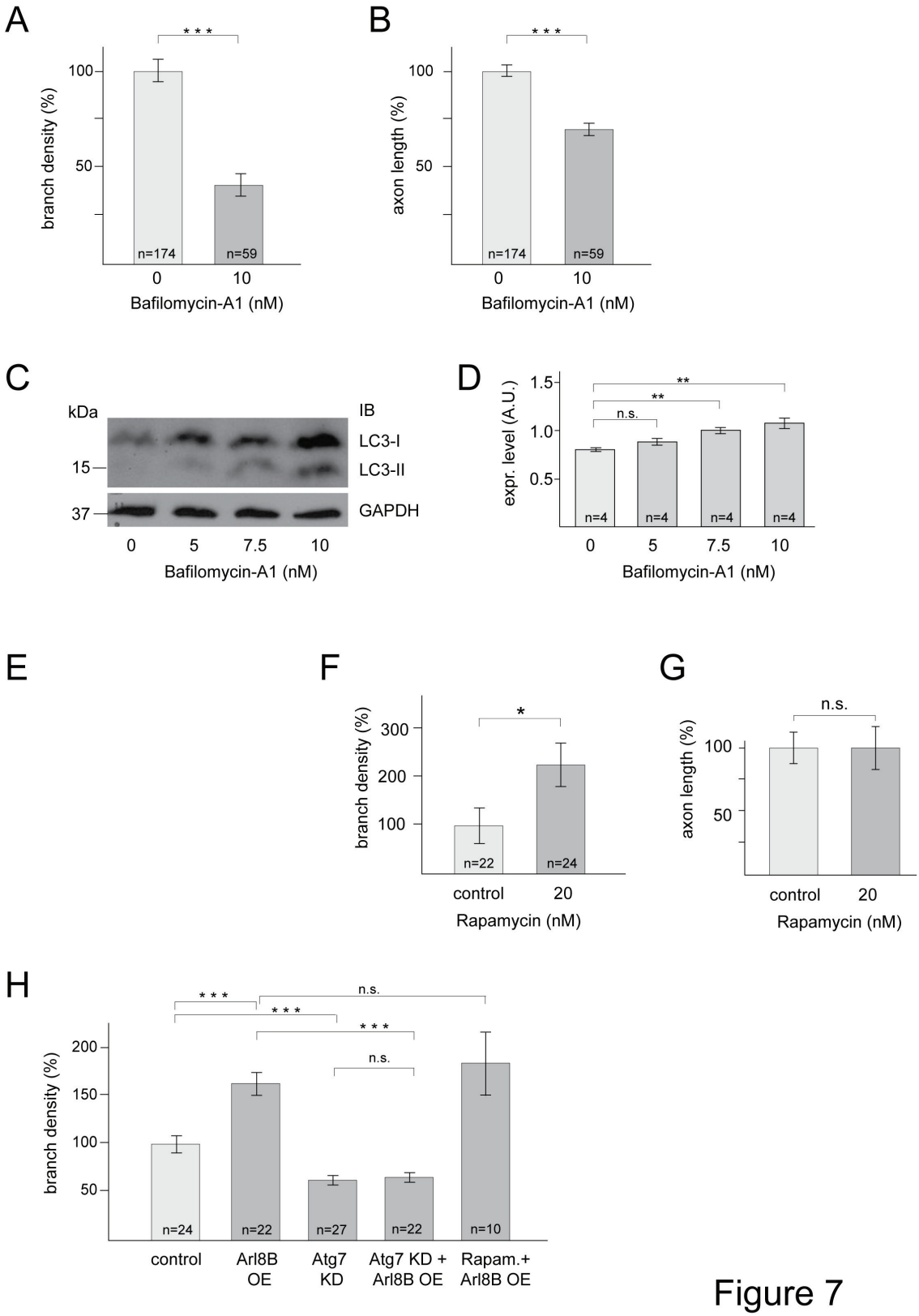

Figure 7

JNeurosci Accepted Manuscript

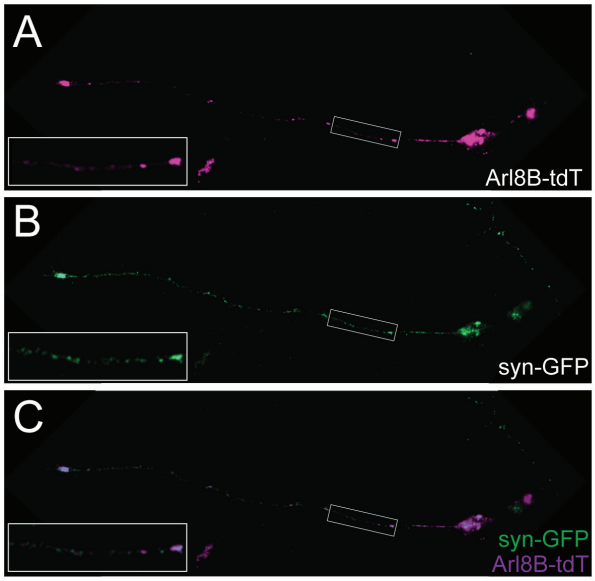

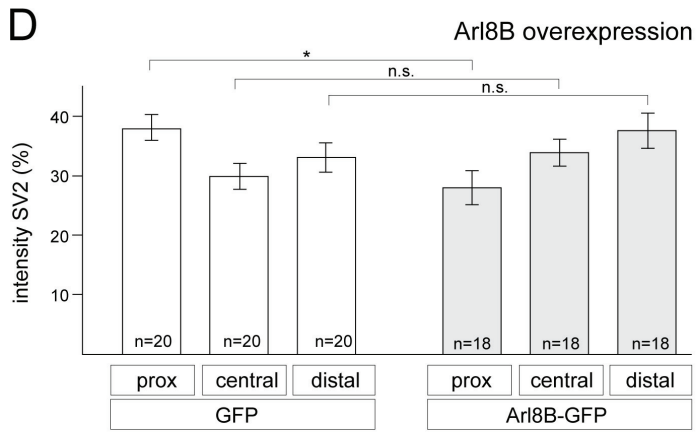

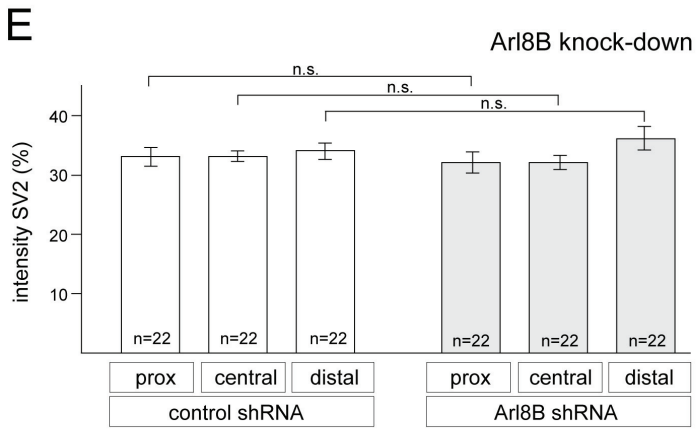

Figure 8

JNeurosci Accepted Manuscript

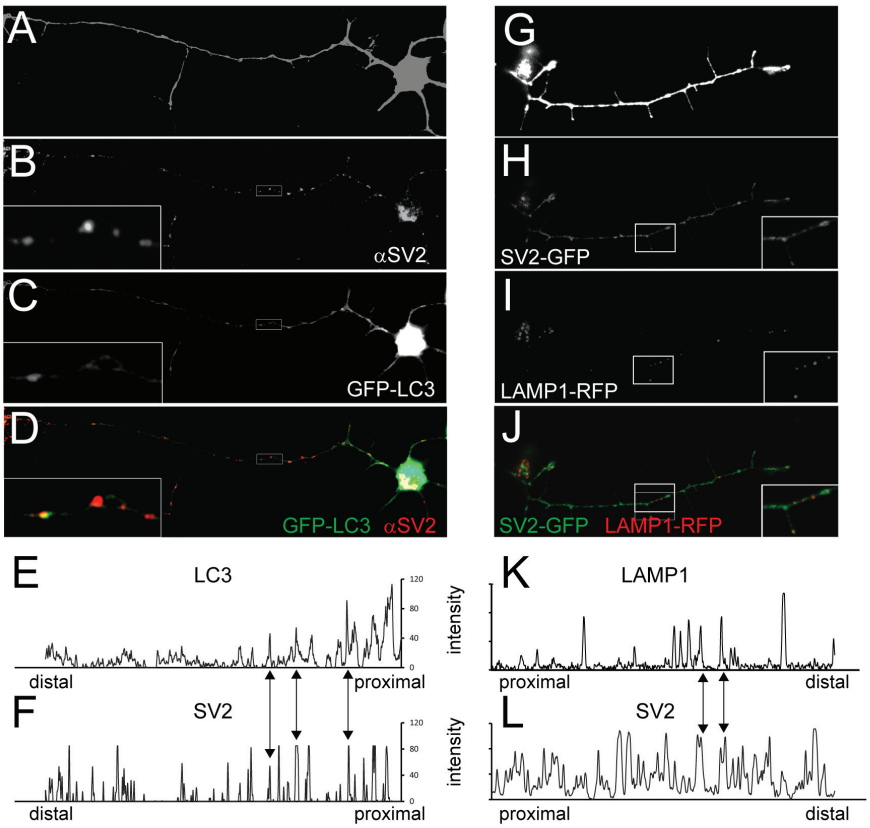

Figure 9

JNeurosci Accepted Manuscript

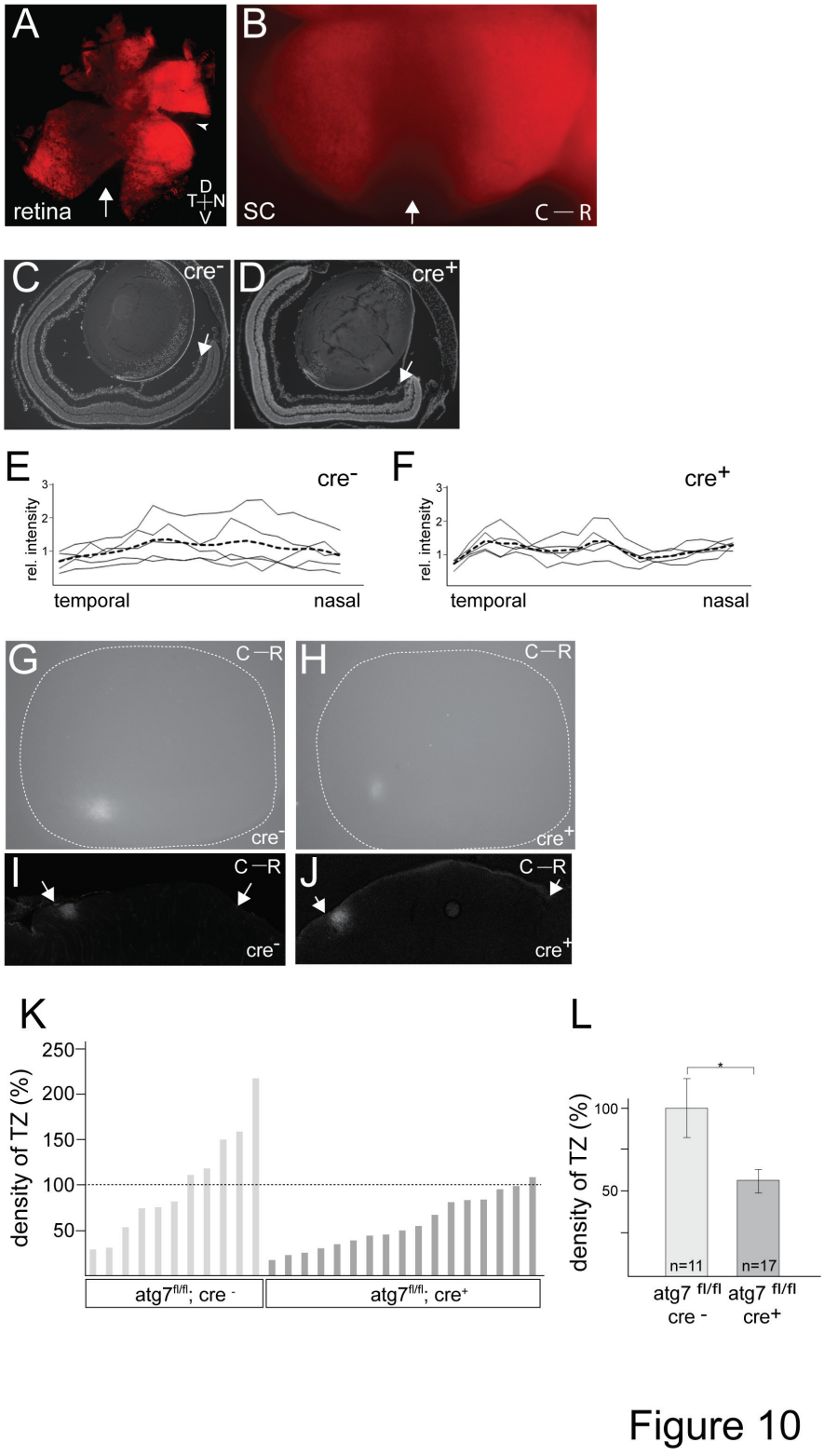

Figure 10

JNeurosci Accepted Manuscript

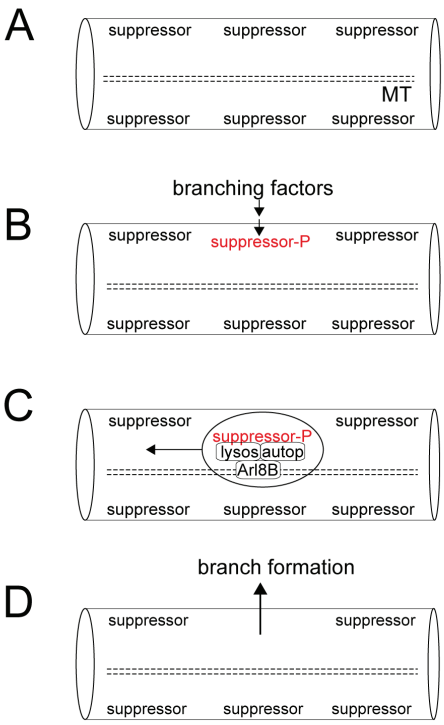

Figure 11